Routledge
Taylor & Francis Group

Check for updates

Age-structured social interactions enhance radicalization

Yao-Li Chuang[a,b], Tom Chou[a,c], and Maria R. D'Orsogna[a,b]

[a]Department of Biomathematics, UCLA, Los Angeles, CA, USA; [b]Department of Mathematics, CSUN, Los Angeles, CA, USA; [c]Department of Mathematics, UCLA, Los Angeles, CA, USA

ABSTRACT

Disaffected youth are among the most susceptible in espousing extremist ideals, as confirmed by demographic studies. We study age-dependent radicalization via a three-stage model where individuals progress through non-radical, activist, and radical states while also aging. Transitions are modeled as age-dependent interactions that are maximized for individuals of the same age and that are enhanced at early adulthood. For comparison, we also derive the age-independent formulation corresponding to our model. We find that age dependence enhances radicalization and leads to waves of radical behavior ebbing and flowing over generational cycles, realizing well-known sociological paradigms. While government intervention is most effective when the appropriate ages are targeted, whether preventive or corrective action is preferable depends on the aggressiveness of the radicalization process.

Introduction

Understanding why and how individuals adopt extremist views has become a prime focus for governments and society. The process, commonly known as "radicalization," is gradual, unfolds through several phases, and may be strongly influenced by social, economic, and cultural factors (McCauley & Moskalenko, 2008; Silber & Bhatt, 2007; Silke, 2008; Sprinzak, 1991). The making of a radical often starts from a state of discontent and feelings of alienation. Mainstream political, social, or religious tenets are gradually rejected and replaced by alternate and increasingly extreme ideologies (Horgan, 2008; King & Taylor, 2011; Koehler, 2014; Silke, 2003). As new ideals become entrenched, a phase of intolerance toward the beliefs, identities, and lifestyles of "others" ensues, accompanied by a proselytizing push (Von Knop, 2007). Finally, radicalization may culminate with the execution of violent, self-destructive acts aimed at spreading terror and damage (Crenshaw, 2011; Meeus, 2015). Although the boundaries between the above-described stages are somewhat fluid, we may succinctly describe radicalization as a sequence of pre-radicalization, self-identification, indoctrination, commitment, and jihadization steps, each being marked by an increasing level of fanaticism (Borum, 2003; Klausen, Campion, Needle, Nguyen, & Libretti, 2016; Moghaddam, 2005; Precht, 2007; Sageman, 2008; Wiktorowicz, 2004).

Radical tendencies can arise at any age, and factors that are traditionally associated with desistance from deviant behavior, such as marriage, career, and education, are not always sufficient deterrents against extremism (King & Taylor, 2011; Sageman, 2004). Disenfranchised young adults, however, are particularly vulnerable to indoctrination and radicalization, especially when their formative years are spent without purpose, education, or positive role models (Lofland & Stark, 1965; Meeus, 2015). Joining extremist groups can provide a sense of belonging and a haven where ideals are shared with like minded individuals (Bakker, 2006; Hart, Atkins, Youniss, & Science, 2005; Loza, El Fatah, Prinsloo, Hesselink-Louw, & Seidler, 2011; Sageman, 2004; Seul, 1999). Today, this is sometimes the case for marginalized immigrant or second-

CONTACT Maria R. D'Orsogna ✉ dorsogna@csun.edu

Color versions of one or more of the figures in the article can be found online at www.tandfonline.com/gmas.

generation youth in western cities, for those growing up in refugee camps, and for right-wing extremists (Doosje, Loseman, & Van Den Bos, 2013; Koehler, 2014). Lacking prospects or motivation, an aversion for the majority and a desire to undermine authority gradually takes root with radicalism providing a sense of purpose and community.

Several mathematical models have been proposed to describe radicalization, both as a general phenomenon (Camacho, 2013; Castillo-Chavez & Song, 2003; Marvel, Hong, Papush, & Strogatz, 2012; Short, McCalla, & D'Orsogna, 2017) and as applied to actual situations, such as the emergence of separatist movements in the Basque country (Ehrhardt, Peco, Tarazona, Villanueva, & Villanueva-Oller, 2013), or of right-wing groups in Germany (Deutscha & Ehrhard, 2015). These models include temporal and in some cases spatial patterns of populations evolving through stages of increasing fanaticism (Ahmed, Audu, Loza, & Maximenco, 2013; Bakker, 2006; Loza et al., 2011; Sageman, 2004). In some instances, field data was used to recapitulate violent incidents that were later used for parameter estimation (Santonja, Tarazona, & Villanueva, 2008). Despite the many useful insights provided, none of these studies include age-sensitive responses to propaganda, emulation of peers and societal pressure. As described above, radicalization is highly age dependent, and developing age-structured models may shed new light on the mechanisms that lead to the establishment of radical groups and help identify optimal intervention strategies.

In this paper, we propose an age-structured model for radicalization where a sequence of stages marked by increasing fanaticism is coupled with age-differentiated interactions. Age dependence intensifies interactions among peers, enhancing the progression toward extremist behavior. Our results suggest that conventional age-independent population models may oversimplify the complexity of social interactions. In some parameter regimes, we find that age structure leads to enhanced radicalization, and that for societies that are highly prone to irreversible radicalization, generational cycles of extremism may arise, realizing a well-known paradigm in political science of alternating decades of ebbing and flowing radicalization (Rapoport, 2002). We also study the effects of government intervention and find that strategically focusing resources on specific age ranges may lead to optimal results.

The model

Several classifications have been introduced in the literature to describe the number of stages between pre-radicalization and full-fledged extremism (Borum, 2003; King & Taylor, 2011; McCauley & Moskalenko, 2008; Moghaddam, 2005; Precht, 2007; Sageman, 2008; Silber & Bhatt, 2007; Wiktorowicz, 2004). In this work, for simplicity, we consider three distinct stages of fanaticism labeled as $i = 0, 1, 2$. The first $i = 0$ stage is that of pre-radicalization, where individuals do not respond to extreme ideologies and are referred to as "non-radicals." Upon being exposed to radical ideas, non-radicals may choose to espouse them, become "activists," and recruit others to their newly found ideology. This intermediate $i = 1$ state corresponds to self-identification and early indoctrination. Finally, $i = 2$ is the last stage whereby activists turn into "radicals" who embrace violence to further their cause. The transitions among the three stages are illustrated in Figure 1.

To introduce an age structure, we define non-radical, activist, and radical population densities $\rho_i(t, a)$ of age a at time t. Transitions from the non-radical $i = 0$ to the activist $i = 1$ pool for individuals of age a
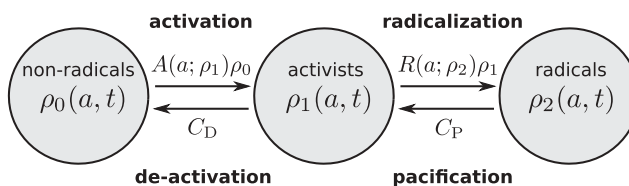

Figure 1. Illustration of the population exchange among non-radicals ρ_0, activists ρ_1, and radicals ρ_2. Activation and radicalization are assumed to occur through social interactions between converting and converted population fractions. De-activation and pacification are proportional to the converted population fractions.

are mediated by the activation rate $A(a; \rho_1)$ that we assume depends on a and on the age structure of the influencing pool ρ_1. Similarly, transitions from the activist $i = 1$ to the radical $i = 2$ population at age a are driven by the radicalization rate $R(a; \rho_2)$. We finally include a de-activation rate C_D that leads individuals to regress from $i = 1$ to $i = 0$ and a pacifying rate C_P for individuals to revert from $i = 2$ to $i = 1$. Both C_D and C_P could be age structured, but we keep them uniform for simplicity. Numerical studies with monotonically increasing $C_D(a)$ and $C_P(a)$ do not yield qualitatively different results and are not shown here. We write our model as

$$\frac{\partial \rho_0}{\partial t} + \frac{\partial \rho_0}{\partial a} = -A(a; \rho_1)\rho_0 + C_D \rho_1, \tag{1}$$

$$\frac{\partial \rho_1}{\partial t} + \frac{\partial \rho_1}{\partial a} = A(a; \rho_1)\rho_0 - \left[C_D + R(a; \rho_2)\right]\rho_1 + C_P \rho_2. \tag{2}$$

$$\frac{\partial \rho_2}{\partial t} + \frac{\partial \rho_2}{\partial a} = R(a; \rho_2)\rho_1 - C_P \rho_2. \tag{3}$$

Equations 1–3 are of the McKendrick-von Foerster type (Chou & Greenman, 2016; Keyfitz, 1997; Leslie, 1945, 1948; McKendrick, 1925; Trucco, 1965), where the left-hand side is the total time derivative $\mathrm{d}/\mathrm{d}t = \partial/\partial t + \left(\partial a/\partial t\right)\partial/\partial a$. Provided that age and time are measured in the same unit, the following will hold: $\partial a/\partial t = 1$, and the $\partial/\partial a$ term is associated to "aging". The transition rates $A(a; \rho_1)$ and $R(a; \rho_2)$ on the right-hand side depend explicitly on age and are defined as

$$A(a; \rho_1) = C_A \int_{a_0}^{a_1} K(a, a'; \alpha_A, \sigma_A)\rho_1(t, a')\,\mathrm{d}a', \tag{4}$$

$$R(a; \rho_2) = C_R \int_{a_0}^{a_1} K(a, a'; \alpha_R, \sigma_R)\rho_2(t, a')\,\mathrm{d}a', \tag{5}$$

Equations 4 and 5 indicate that all individuals between ages a_0 and a_1 are able to influence those at age a via the "interaction kernels" $K(a, a', \alpha_j, \sigma_j)$ that we model as

$$K(a, a'; \alpha_j, \sigma_j) = \frac{\exp\left[-\frac{(a-\alpha_j)^2 + (a-a')^2}{2\sigma_j^2}\right]}{\int_{-\bar{a}}^{\bar{a}} \exp\left[-\frac{s^2}{\sigma_j^2}\right] ds} \tag{6}$$

for $j = A, R$, where $\bar{a} \equiv |a_1 - a_0|$. The kernels specify how an individual at age a is influenced by another at age a'. Equation 6 is defined so that if $\rho_1(t, a')$ in Equation 4 is age independent, then $A(a; \rho_1) \to C_A$, and similarly if $\rho_2(t, a')$ is age independent, then $R(a; \rho_2) \to C_R$. The kernels are maximized when $a = \alpha_j$ and when $a = a'$. The former condition expresses that individuals are most susceptible to activation and radicalization when they are at certain "target" ages α_j ($j = A, R$). The latter condition arises from "peer-to-peer" interactions, whereby individuals are most influenced by those of similar age. The interaction kernels in Equation 6 decrease as a shifts away from α_j and when the age gap $|a - a'|$ increases. How quickly these kernels decline is specified by σ_j ($j = A, R$), the spread of the interaction kernel. If σ_j is large, the influence exerted by individuals at age a' on those at age a may persist for large age differences $|a' - a|$, and for large $|a - \alpha_j|$. Conversely, for small σ_j the kernels will be appreciable only for $a \sim a'$ and $a \sim \alpha_j$. Furthermore, with Equation 4, we assume that activation ($i = 0$ to $i = 1$) occurs through age-dependent social interactions between the ρ_0 non-radical and the activist ρ_1 populations; a similar construct holds for radicalization ($i = 1$ to $i = 2$) in Equation 5 through which the ρ_1 activists interact with the ρ_2 radicals. The interaction kernels in Equation 6 indicate that individuals are most susceptible to activation and radicalization at target ages $a = \alpha_j$ for $j = A, R$, respectively, as well as by "peer to peer" interactions with individuals of similar age, but more radicalized. The interaction kernels reach their maximum at $a = \alpha_j$, while peer-to-

peer interactions are maximized at $a = a'$. The age ranges σ_j represent the spread of the interaction kernels. We will study the model defined by Equations 1–6 for a typical age span of $[a_0, a_1]$, so that $\bar{a} \equiv a_1 - a_0$ in the denominator of Equation 6. The latter is introduced to guarantee that upon integration over $[a_0, a_1]$ the kernels are independent of σ_j. This will be useful when deriving the age-independent version of Equations 1–6, since the denominator will yield age-independent transition rates that depend only on the C_j amplitudes and not on σ_j. It is important to note that the presence of the denominator implies that the total area under the kernel is unity; kernels with a higher σ_j will be wider but shallower than kernels with a lower σ_j.

The chosen $[a_0, a_1]$ boundaries specify the range for effective age-based interactions: individuals of age $a < a_0$ are too young to influence or be influenced by an ideology or by their peers, and those with age $a > a_1$ may be too old or entrenched for change. The age boundaries also imply that Equations 1–6 represent radicalization across a single generation, beginning at a_0 and ending at a_1. For simplicity, we assume that within $[a_0, a_1]$ death is negligible. To complete our model, we must include boundary conditions that are chosen at $a = a_0$ as

$$\rho_0(t, a_0) = \sum_{i=0,1,2} \rho_i(t, a_1), \tag{7}$$

$$\rho_1(t, a_0) = \rho_2(t, a_0) = 0. \tag{8}$$

The above conditions imply that the total population exiting from age $a = a_1$, including radicals, activists, and non-radicals, will re-enter the system at age a_0 as non-radical. The model is now complete as Equations 1–3 are advection-reaction equations that require boundary conditions only on one side of the domain. Our basic assumption is that at each $i = 0, 1, 2$ stage, the population is large and stochastic effects can be neglected, justifying the use of deterministic, mean-field McKendrick-von Foerster type equations (Chou & Greenman, 2016; Keyfitz, 1997; Leslie, 1945, 1948; Trucco, 1965). We also neglect birth and death events for simplicity, assuming a constant total population and focusing on how this constant population is distributed across ages and radicalization stages in response to different social interaction mechanisms.

Finally, we introduce the size of the population at stage i between ages a_1 and a_2 at time t as $N_i(t; [a_1, a_2]) \equiv \int_{a_1}^{a_2} \rho_i(t, a) \, da$, a quantity that will be invoked in the next section. Unless otherwise stated, we will consider initial conditions such that $\rho_0(0, a) \gg \rho_1(0, a) \simeq \rho_2(0, a) > 0$, to mimic a society where the majority of the population is initially non-radical. Note that because of the structure of Equations 1–3, $\rho_1(0, a)$ and $\rho_2(0, a)$ must be non-zero to induce activation and radicalization.

Results

We begin by deriving the age-independent equations corresponding to Equations 1–3. These will give us a benchmark against which the full, age-structured model will be later compared and contrasted to. What we will obtain is an ODE system where kernels and transition rates are condensed in an age-uniform quantity. Comparing results from both formulations will be useful to understand what features we fail to capture when neglecting age structure.

A. Age-independent model and stationary solutions

To construct the age-independent version of our model, we define the fractional populations $n_i(t)$ as

$$n_i(t) \equiv \frac{\displaystyle\int_{a_0}^{a_1} \rho_i(t, a) \, da}{\displaystyle\sum_{i=0,1,2} N_i(t; [a_0, a_1])} \tag{9}$$

where the denominator $N \equiv \sum_{i=0,1,2} N_i(t; [a_0, a_1])$ represents the entire population between ages a_0 and a_1. The resulting N is time independent due to population conservation. By construction $0 \leq n_i(t) \leq 1$ for all i and $\sum_{i=0,1,2} n_i(t) = 1$. We now let $\sigma_j \to \infty$ in Equation 6 for $j = A, R$. The interaction kernels become constants and the age-independent transition rates can be rewritten as $A(\rho_1) = C_A \int_{a_0}^{a_1} \rho_1(t, a) \, da/(2\bar{a}) = N C_A n_1(t)/(2\bar{a})$, and $R(\rho_1) = C_R \int_{a_0}^{a_1} \rho_2(t, a) \, da/(2\bar{a}) = N C_R n_2(t)/(2\bar{a})$. Finally, integrating Equations 1–3 over the ages between a_0 and a_1 and dividing the results by N, we find that the interactions factor as

$$\frac{dn_0}{dt} = -c_A n_0 n_1 + c_D n_1, \tag{10}$$

$$\frac{dn_1}{dt} = c_A n_0 n_1 - c_D n_1 - c_R n_1 n_2 + c_P n_2, \tag{11}$$

$$\frac{dn_2}{dt} = c_R n_1 n_2 - c_P n_2, \tag{12}$$

where $c_A \equiv N C_A/(2\bar{a})$, $c_R \equiv N C_R/(2\bar{a})$, $c_D \equiv C_D$, and $c_P \equiv C_P$. Note that there is no equivalent to the boundary conditions Equations 7 and 8 since we integrated out age dependence. Equations 10–12 form a degenerate system, which, by substituting $n_1 = 1 - n_0 - n_2$, reduces to

$$\frac{dn_0}{dt} = (1 - n_0 - n_2)(c_D - c_A n_0), \tag{13}$$

$$\frac{dn_2}{dt} = n_2 [c_R(1 - n_0 - n_2) - c_P]. \tag{14}$$

The model defined by Equations 13 and 14 is similar to previous multi-compartment models where extremism increases due to interactions between radicals and non-radicals (Castillo-Chavez & Song, 2003; Deutscha & Ehrhard, 2015; Short et al., 2017). By invoking the Bendixson-Dulac theorem (Burton, 2005; Dumortier, Llibre, & Artés, 2006) with $1/[n_2(1 - n_0 - n_2)]$ as the Dulac function, it can be shown that limit cycles do not arise. All trajectories converge to fixed points (n_0^*, n_2^*) as shown in Figures 2 and 3. Note that all fixed points must satisfy the constraint $0 \leq n_i^* \leq 1$ for all i. Sociologically, within some radical groups, pacification may be rare due to extreme die-hard fanaticism, while in other groups, gradually retracting from radicalization may be possible. The reversibility of the final, radical stage (i.e., whether $c_P = 0$ or $c_P > 0$) plays a key role in determining qualitative behaviors as observed in opinion dynamics models (Verma, Swami, & Chan, 2014; Waagen, Verma, Chan, Swami, & D'Souza,
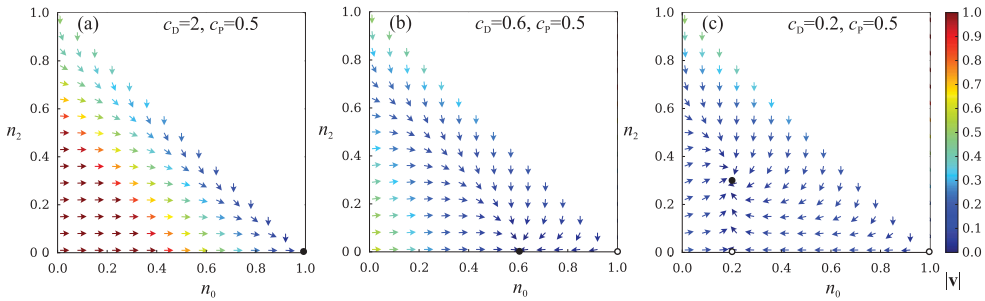
Figure 2. Reversible radicalization phase portraits derived from Equations 13 and 14 for three values of c_D and fixed $c_P = 0.5$, $c_A = c_R = 1$. The magnitude of the phase flow $\mathbf{v} \equiv (dn_0/dt, dn_2/dt)$ is color coded. (a) For $c_D/c_A > 1$ all trajectories converge to the stable fixed point at $(n_0^*, n_2^*) = (1, 0)$ denoted by a solid circle. (b) For $1 - c_P/c_R < c_D/c_A \leq 1$ the stable fixed point is $(n_0^*, n_2^*) = (c_D/c_A, 0)$ while $(1, 0)$ turns unstable and is denoted by an open circle. (c) Finally, for $c_D/c_A \leq 1 - c_P/c_R$ the sole stable solution is $(n_0^*, n_2^*) = (c_D/c_A, 1 - c_D/c_A - c_P/c_R)$, while the other two are unstable. The regions above $n_0 + n_2 = 1$ are unphysical as $0 \leq n_i \leq 1$ for $i = 0, 1, 2$ by construction.
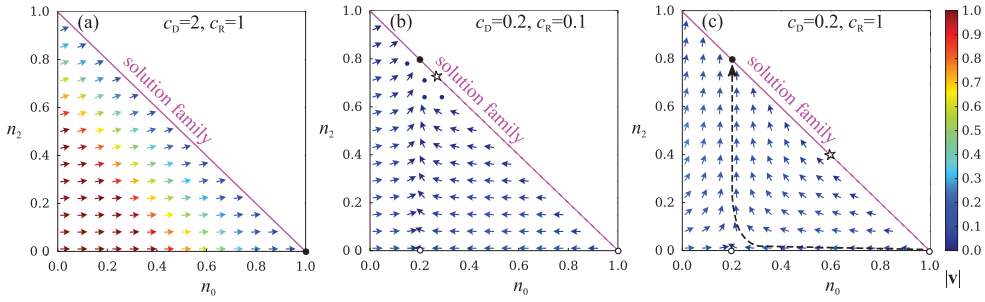
Figure 3. Irreversible radicalization phase portraits derived from Equations 13 and 14 for three sets of (c_D, c_R) and fixed $c_P = 0$, $c_A = 1$. A family of solutions $n_0^* + n_2^* = 1$ (depicted in magenta) arises in addition to the three fixed points. (a) For $c_D/c_A > 1$, the solution family and so the fixed point $(1, 0)$ are marginally stable. (b)–(c) For $c_D/c_A \leq 1$, the portion of the solution family that satisfies $n_0^* > (c_D + c_R)/(c_A + c_R)$ becomes unstable (dashed magenta line), along with the fixed points $(1, 0)$ and $(c_D/c_A, 0)$. The remainder of the solution family and the fixed point $(c_D/c_A, 1 - c_D/c_A)$ are marginally stable (solid magenta line). In panel (b) where $c_R = 0.1$ the stable portion of the solution family is smaller than in panel (c) where $c_R = 1.0$. Phase flows steer trajectories toward the solution family, avoiding the stable fixed point. A trajectory starting near $(1, 0)$ and ending at $(c_D/c_A, 1 - c_D/c_A)$ is depicted in panel (c) as a black dashed curve. Other trajectories may end anywhere along the stable portion of the solution family.

2015). Hence, in analyzing Equations 13 and 14, we consider two distinct cases: reversible radicalization, whereby $c_P > 0$, and irreversible radicalization, whereby $c_P = 0$.

If $c_P > 0$ and radicalization is reversible, a maximum of three fixed points may arise, as shown in Figure 2(a–c). The fixed point at $(n_0^* = 1, n_2^* = 0)$ (and $n_1^* = 0$), where all individuals are non-radical. This fixed point corresponds to "utopia," a society without any activists or radicals. The second fixed point is the "dormant" state $(n_0^* = c_D/c_A, n_2^* = 0)$ (and $n_1^* = 1 - c_D/c_A$), characterized by the presence of activists who do not turn radical. Here, the non-radical population n_0^* is given by balancing the c_D de-activation-induced influx and the c_A activation-induced efflux, yielding $n_0^* = c_D/c_A$. Finally, the third "turmoil" fixed point is at $(n_0^* = c_D/c_A, n_2^* = 1 - c_D/c_A - c_P/c_R)$ (and $n_1^* = c_P/c_R$), where a non-zero fraction of the population is permanently radicalized. While the fraction of the non-radical population is again given by $n_0^* = c_D/c_A$, the activist population is similarly determined by balancing the c_P pacification-induced influx and the radicalization-induced efflux c_R, yielding $n_1^* = c_P/c_R$. The existence and stability of these fixed points depend on the values of c_D/c_A and c_P/c_R as well as whether they satisfy the $0 \leq n_i^* \leq 1$ constraints.

When de-activation dominates activation and $c_D/c_A > 1$ utopia is the only feasible steady state. The phase portrait of the system is shown in Figure 2(a): all trajectories converge to $(1, 0)$. Upon increasing activation so that $1 - c_P/c_R < c_D/c_A \leq 1$, the dormant state enters the physical domain and becomes the only stable solution. The phase portrait in Figure 2(b) shows that all trajectories converge to $(c_D/c_A, 0)$, while $(1, 0)$ becomes a saddle point. Finally, when activation dominates de-activation and $c_D/c_A \leq 1 - c_P/c_R$, turmoil replaces the dormant state as the only stable solution. Figure 2(c) shows all trajectories converging to $(c_D/c_A, 1 - c_D/c_A - c_P/c_R)$, while the other two fixed points become saddle nodes.

Under irreversible radicalization, when $c_P = 0$, in addition to the above fixed points, a family of solutions $n_0^* + n_2^* = 1$ (and $n_1^* = 0$) will arise. This follows from the irreversible nature of radicalization: in the absence of a pacification mechanism, the n_2 radical group becomes a sink, eventually depleting the n_1 activist pool. As a consequence, population exchanges between n_0 and n_2 are interrupted, stranding phase trajectories along the $n_0^* + n_2^* = 1$ line. Note that when $c_P = 0$, the stability interval for the dormant state, $1 - c_P/c_R < c_D/c_A \leq 1$ vanishes, so that the dormant state is always unstable. Under irreversible radicalization, increases in c_A shift the system from utopia directly to turmoil.

In Figure 3(a), we plot the phase portrait for $c_D/c_A > 1$; the fixed point $(1, 0)$ and the solution family $n_0^* + n_2^* = 1$ are both marginally stable. In Figure 3(b,c) we set $c_D/c_A \leq 1$ and consider different values of c_R. In both figures, the fixed point $(c_D/c_A, 1 - c_D/c_A)$ is marginally stable while

$(1, 0)$ is unstable. The segments of the solution family $n_0^* + n_2^* = 1$ between $(1, 0)$ (open circle) and $((c_D + c_R)/(c_A + c_R), 1 - (c_D + c_R)/(c_A + c_R))$ (open star) become unstable. Because of the irreversibility of radicalization, the dynamics are highly sensitive to initial conditions; where a trajectory will end along the stable portion of the $n_0^* + n_2^* = 1$ line depends on where the trajectory starts. An important role is also played by the radicalization rate c_R. As the latter increases, the open star $((c_D + c_R)/(c_A + c_R), 1 - (c_D + c_R)/(c_A + c_R))$ will shift toward $(1, 0)$, expanding the stable portion of the solution family. Larger c_R values, as shown in Figure 3(c), enhance the stability of the solution family, as trajectories are steered more vigorously toward $n_0^* + n_2^* = 1$, before turmoil can be reached.

The above analysis reveals that three steady states are possible within the age-independent formulation of model: utopia, a dormant state, and turmoil, as summarized in Figure 4. Under reversible radicalization, the system settles into one of the three depending on the values of c_D/c_A and c_P/c_R, while for irreversible radicalization, the final steady state also depends on initial conditions.

B. Full age-dependent model

We now consider the full age-dependent model as defined in Equations 1–6, starting with the scenario of reversible radicalization, $C_P > 0$. As shown in Figure 2, the corresponding age-independent model progresses through the utopia, dormant, and turmoil steady states as c_D decreases. To compare results, we begin by examining the steady states arising from the age-dependent model by varying C_D while fixing other parameters. We assume the radicalization window to occur between ages $a_0 = 5$ and $a_1 = 55$; to include age dependence, we must also specify α_j and σ_j. For simplicity, we assume the same age dependence for activation and radicalization, setting $\alpha_A = \alpha_R = 20$ years, and $\sigma_A = \sigma_R = 10$ years. We assume initial conditions $\rho_0(a, 0) = 0.989$, $\rho_1(a, 0) = 0.01$, and $\rho_2(a, 0) = 0.001$, representing an overwhelmingly non-radical society. Finally, we choose $C_A = C_R = 2$, $C_P = 0.5$. The initial conditions yield a total population $N = \bar{a}$, leading to the corresponding parameter values $c_A = c_R = 1$, $c_P = 0.5$ for the age-independent model, which are exactly the same values used in Figure 2. Since $c_D = C_D$ we finally select $C_D = 2$, 0.6, and 0.2, so that full comparisons can be made with Figure 2 and the implications of including age dependence in the model can be highlighted. Within the age-dependent scenario, analytical estimates of steady states are not available, and numerical simulations must be run for every set of chosen parameters. Henceforth, all times and age units will be assumed to be years. All main parameters and terms are summarized in Table 1.
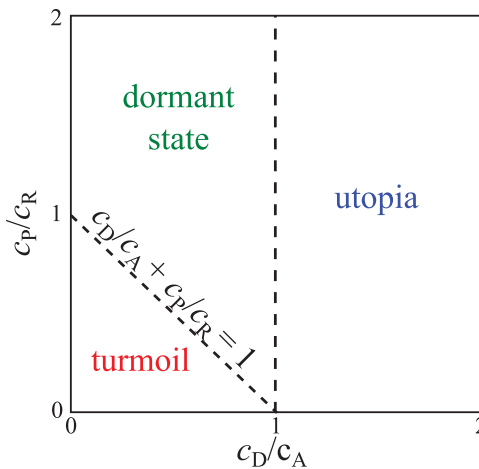

Figure 4. Phase diagram of the age-independent model under reversible radicalization. For $c_D \geq c_A$, the system settles at utopia $(n_0^* = 1, n_1^* = 0, n_2^* = 0)$. For $c_D < c_A$ and $c_D/c_A + c_P/c_R \geq 1$, the dormant state is stable at $(n_0^* = c_D/c_A, n_1^* = 1 - c_D/c_A, n_2^* = 0)$. For $c_D/c_A + c_P/c_R < 1$, the system is in turmoil at $(n_0^* = c_D/c_A, n_1^* = c_P/c_R, n_2^* = 1 - c_D/c_A - c_P/c_R)$.

Table 1. List of parameters and functional forms used in the model presented in Eqs. 1–6. Government intervention quantities are discussed in Section IV.

Symbol	Description	Values
$A(a; \rho_1)$	activation rate coefficient	Eq. (4)
$R(a; \rho_2)$	radicalization rate coefficient	Eq. (5)
G	government conversion rate coefficient	Eq. (22)
C_A	activation intensity	1 – 12
C_R	radicalization intensity	0 – 20
C_D	de-activation intensity	0.2 – 5
C_P	pacification intensity	0 – 0.5
C_G	government intervention intensity	0–1
α_A	activation targeted age	20 ys.
α_R	radicalization targeted age	20 ys.
α_G	government targeted age	20 ys.
a_0	lower bound of interaction age window	5 ys.
a_1	upper bound of interaction age window	55 ys.
σ_A	activation age breadth	10 ys.
σ_R	radicalization age breadth	10 ys.
σ_G	government intervention age breadth	10 ys.
μ	fraction of intervention on activists	0 – 1

In Figure 5, we numerically evaluate Equations 1–6 for $t = 100$ and plot the $n_1(t)$ activist and $n_2(t)$ radical populations as defined by Equations 9. For comparison, we also show the corresponding age-independent $n_1(t), n_2(t)$ populations obtained from Equations 10–12 where initial conditions were specified as $n_0(0) = 0.989$, $n_1(0) = 0.01$, and $n_2(0) = 0.001$ for consistency. For $C_D = 2$ the age-independent model predicts utopia, a result that is confirmed in the age-dependent case. We do not plot the dynamics corresponding to this case, since both $n_1(t)$ and $n_2(t)$ quickly vanish in both formulations. For $C_D = 0.6$, Figure 5(a) shows that a small but nonzero radical fraction $n_2(t \to \infty)$ emerges within the age-dependent model, in contrast to the age-independent prediction of a dormant state whereby $n_2^* = 0$. This discrepancy is due to age-enhancement of the activation $A(a; \rho_1)$ and radicalization $R(a; \rho_2)$ rates near the early ages $a \simeq \alpha_j$ for $j = $ A, R respectively. Recall that by construction, and as discussed when justifying the shape of the sensitivity kernels in Equation 6, enhancing the transition rates at a given age, necessarily decreases them at other age intervals. Here, increasing the transition rates around α_j is sufficient to drive the system toward turmoil, despite the same transition rates being lowered in other age windows.

Finally, for $C_D = 0.2$, both the age-dependent and age-independent models reach turmoil as shown in Figure 5(b). Note that the steady-state activist and radical fractions arising from the age-dependent model, $n_1(t \to \infty) = 0.36$ and $n_2(t \to \infty) = 0.21$, are lower than the predicted $n_1^* = 0.5$ and $n_2^* = 0.3$ values in the age-independent case; this is due to the age structure of the kernel in Equation 6. In the age-independent case, where the transition rates c_A and c_R are not age structured, the chosen parameters lead to turmoil where only a relatively small population is non-radical: $n_0^* = 1 - n_1^* - n_2^* = 0.2$. The age-dependent formulation allows for age variability in the transition rates $A(a; \rho_1)$ and $R(a; \rho_2)$, which increase at the peak ages α_A and α_R, but decrease for other ages. The local increases in $A(a \simeq \alpha_A; \rho_1)$ and $R(a \simeq \alpha_R; \rho_2)$ do not appreciably raise the number of activists or radicals compared to those in the turmoil state of the age-independent formulation, since they are already sustained. Decreasing the transitions in other age windows, however, stymies the radicalization of other individuals far from the peak age, resulting in an overall net decrease of the radical and activist populations so that $n_1(t \to \infty) < n_1^*$ and $n_2(t \to \infty) < n_2^*$.

In Figure 5(c), we select $C_A = C_R = 2$, $C_D = 0.9$, and $C_P = 0.05$ to yield the age-independent, turmoil steady state ($n_0^* = 0.9, n_1^* = 0.05, n_2^* = 0.05$), with a large non-radical population. In the age-dependent model, enhanced rates at the peak ages α_A and α_R allow for the transition of a much larger non-radical population into the activist and radical pools, compared to the case discussed in Figure 5(c) where the non-radical population was small. Overall, a larger value for $n_2(t \to \infty) = 0.11$ is observed in the age-dependent formulation than in the age-independent one. Note that in Figure 5(b,c),
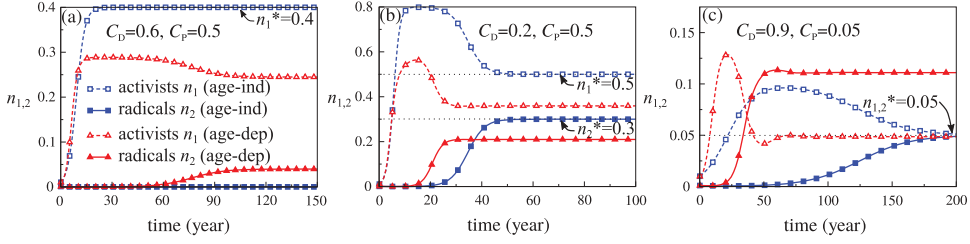
Figure 5. Time dependence of the the activist n_1 and radical n_2 population fractions from the age-independent and age-dependent formulations of our model. We fix $C_A = C_R = 2$ in all panels and set $C_D = 0.6$ and $C_P = 0.5$ in panel (a); $C_D = 0.2$ and $C_P = 0.5$ in panel (b) and $C_D = 0.9$ and $C_P = 0.05$ in panel (c). Additional parameters for the age-dependent model are set to $\alpha_A = \alpha_R = 20$, $\sigma_A = \sigma_R = 10$. Initial conditions are $(\rho_0(a, 0), \rho_1(a, 0), \rho_2(a, 0)) = (0.989, 0.01, 0.001)$. In panel (a), age dependence allows a small fraction of radicals to rise, while the age-independent model predicts a dormant state at $(n_0^* = 0.6, n_1^* = 0.4, n_2^* = 0)$. In panels (b) and (c), both models evolve toward turmoil. In panel (b) the age-independent model predicts aggressive radicalization with turmoil at $(n_0^* = 0.2, n_1^* = 0.5, n_2^* = 0.3)$; including age-structure leads to a lower radical fraction. Radicalization is less aggressive in panel (c). Here, the age-independent turmoil steady state is at $(n_0^* = 0.9, n_1^* = 0.05, n_2^* = 0.05)$, and age dependence increases the radical population. Note that in all panels, age dependence accelerates activist and radical growth, regardless of the final steady states.

activists and radicals emerge earlier in the age-dependent than in the age-independent model, regardless of the final steady state. This trait persists for several parameter choices, suggesting that age-structured rates accelerate radicalization, due to their enhancement at young ages.

In Figure 6, we plot the age-structured distributions for activists and radicals $\rho_1(a, t \rightarrow \infty)$ and $\rho_2(a, t \rightarrow \infty)$ as approximated at $t = 100$ after steady state has been reached. In Figure 6(a), we use the same parameters as in Figure 5(a) where the age-independent model predicts a dormant state. Here, the age-structured steady state population is mostly in the activist state, peaking at age $a \simeq 21$, although a small fraction of radicals $\rho_2(a, t \rightarrow \infty)$ emerges and peaks at age $a \simeq 23$, due to the locally increased transition rates, as described above. Note that the maximum in $\rho_1(a, t \rightarrow \infty)$ occurs at age $a^* > \alpha_A$. This can be explained by noting that the greatest transition toward the activist state occurs at age α_A, when the sensitivity kernel $K(a, a', \alpha_A, \sigma_\alpha)$ reaches its maximum. The individuals who joined the activist group at age α_A will age and remain, at least for some time, in this state before transitioning to the radical or non-radical states for ages $a > \alpha_A$. Additional individuals will join the activist pool at older ages, yielding a cumulative activist population that is greatest for $a^* > \alpha_A$, as $\rho_1(a^*, t \rightarrow \infty)$ contains individuals that transitioned earlier and aged while remaining in the activist state, but also those who transitioned later. At older ages, the kernel in Equation 6 decreases: individuals leave the activist pool in larger numbers than they will join it, so that $\rho_1(a, t \rightarrow \infty)$ decreases from its maximum. A similar argument can be applied to $\rho_2(a, t \rightarrow \infty)$ that also peaks at age $a > \alpha_R$.

A more interesting case is shown in Figure 6(b) where the chosen parameters are the same as in Figure 5(b) and where the deactivation rate C_D is lower than what used in Figure 6(a). In this case, the corresponding age-independent model reaches a strong turmoil steady state. We observe that the radical population in Figure 6(b) peaks near $a \simeq 23$, while activists are bimodally distributed, peaking at both younger $a \simeq 13$ and older ages $a \simeq 35$. Of the two $\rho_1(a; t \rightarrow \infty)$ maxima, the first occurs at age $a < \alpha_A$. Here, due to the low value of C_D, a large activist population rapidly emerges at young ages; these individuals gradually transition toward the radical stage and further increase $R(a; \rho_2)$. Eventually, the radicalized population becomes so numerous that $R(a; \rho_2)$ overtakes the activation rate $A(a; \rho_1)$, causing activists to vigorously transition to the radical pool, effectively leading to the net loss of activists around age $a \simeq \alpha_A$ as seen in Figure 6(b). The first peak in $\rho_1(a, t \rightarrow \infty)$ thus emerges at younger ages $a < \alpha_A$, when the number of radicals is relatively low and so is $R(a; \rho_2)$. At intermediate ages $a > \alpha_A$, $R(a; \rho_2)$ begins to decline along with the radical population $\rho_2(a, t \rightarrow \infty)$, leading to an increase in the activist population $\rho_1(a, t \rightarrow \infty)$. These individuals shift to the non-activist pool at a slow rate as C_D is relatively low. As older ages are approached, activation further decreases, $\rho_1(a, t \rightarrow \infty)$ begins to decline, and
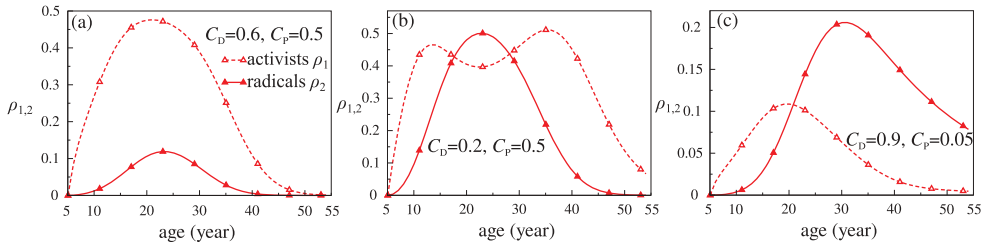
Figure 6. Age distribution of activists and radicals for the parameters used in Figure 5(a–c). Panel (a) shows a small fraction of radicals, deviating from the dormant steady state predicted by the age-independent model. Both activist and radical populations peak at ages slightly larger than a_R. Panel (b), corresponding to strong turmoil, shows the radical population peaking at ages slightly larger than a_R, accompanied by a bi-modal age-distribution of activists. Panel (c) corresponds to mild turmoil and shows a uni-modal age distribution for both radicals and activists, with the radical peak occurring at ages larger than a_A and the activist maximum at ages lower than a_A. The mechanisms that lead to uni-modal or bimodal distributions as well as to the shifts in the peaks compared to a_A are detailed in the text.

individuals increasingly return to the non-radical state. These two competing age-dependent mechanisms give rise to the second peak in $\rho_1(a; t \to \infty)$ as seen in Figure 6(b).

Finally, in Figure 6(c), we show the age dependence of the steady state radical and activist populations using the same parameters as in Figure 5(c), where the age-independent model predicts mild turmoil. We find that activists peak at age $a^* \simeq 19$, while radicals reach their maximum at age $a^* \simeq 28$. The mechanisms driving the observed age-dependent patterns are similar to what described for Figure 6 (b), however here we do not observe a secondary peak for $\rho_2(a, t \to \infty)$. In this case, the de-activation rate $C_D = 0.9$ is larger than what is used in Figure 6(b), where $C_D = 0.2$. As a result, as the radicalization rate $R(a; \rho_2)$ decreases at older ages, the large de-activation rate does not allow for an intermediate activist population to persist; rather, most of the former radicals turn directly to non-radical behavior. The activist population declines continuously in age and does not exhibit a secondary maximum. Upon comparing Figure 6(b,c) we also see that while in the state of strong turmoil, adherents may remain active even at older ages when the number of radical extremists vanishes. On the other hand, panel (c) shows that in cases of mild turmoil, the number of radicals and activists is concentrated at early ages, suggesting that fervor wanes significantly with age.

We now consider the case of irreversible radicalization $C_P = 0$ in Equations 1–6. In the previous subsection, we showed that in the age-independent case, the dynamics is strongly dependent on the radicalization rate; hence, we begin by illustrating the particular case of fixed $C_A = 12$, $C_D = 5$, and varying C_R. We assume the same age parameters as the reversible case above, where $\alpha_A = \alpha_R = 20$ and $\sigma_A = \sigma_R = 10$. Initial conditions are also chosen as above with $\rho_0(a, 0) = 0.989$, $\rho_1(a, 0) = 0.01$, and $\rho_2(a, 0) = 0.001$. Within the age-independent model, the above parameters correspond to $c_A = 6$, $c_D = 2.5$ and $c_R = C_R/2$ and yield a stable turmoil state at $(n_0^* = 5/6, n_1^* = 0, n_2^* = 1/6)$ and an unstable dormant state at $(n_0^* = 5/6, n_1^* = 1/6, n_2^* = 0)$; neither of these configurations depend on c_R.

In Figure 7(b), we increase $C_R = 2$ ($c_R = 1$), while keeping all other parameters unchanged. In the age-independent formulation, the system converges to turmoil at $(n_0^* = 5/6, n_1^* = 0, n_2^* = 1/6)$ after roughly 60 years. The dynamics are quite different in the age-dependent version of the model. Here, the activist fraction $n_1(t)$ rises and declines more abruptly than in the age-independent case; similarly, the radical fraction $n_2(t)$ increases at earlier times and more vigorously, greatly surpassing the $n_2^* = 1/6$ steady state value of the age independent model at long times. Of particular importance is the fact that age-dependent transitions allow the $n_1(t)$ activist population to exist continuously and not vanish as it does in the age-independent case. This non-depleted pool of $n_1(t)$ radicals provides an uninterrupted source of recruits for $n_2(t)$, which can grow to large values; it also provides a pathway for more $n_0(t)$ non-radicals to be initiated into the radicalization process. Indeed, $n_0(t \to \infty) = 0.64$ at steady state in the age-dependent model as opposed to $n_0^* = 5/6 = 0.83$ in the age-independent case. These results

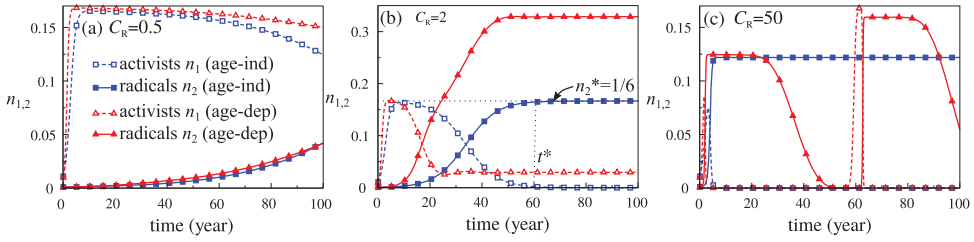**Figure 7.** Time dependence of the activist n_1 and radical n_2 populations from the age-independent and age-dependent formulations of our model. We fix $C_A = 12$ and $C_D = 5$ and set $C_R = 0.5$ in panel (a), $C_R = 2$ in panel (b), and $C_R = 50$ in panel (c). Additional parameters for the age-dependent model are $a_A = a_R = 20$, $\sigma_A = \sigma_R = 10$. Initial conditions are $(\rho_0(a, 0), \rho_1(a, 0), \rho_2(a, 0)) = (0.989, 0.01, 0.001)$. In all panels, the activist population rises first, followed by radical growth. In the age-independent case, $n_1(t), n_2(t)$ saturate either at turmoil as shown in panels (a) (b) or along the solution family as shown in panel (a). Age dependence slightly accelerates the growth of activists and radicals at low C_R in panel (a); greatly enhances the growth of radicals by maintaining a finite activist population at intermediate C_R in panel (b); and leads to activist and radical population oscillations at high C_R in panel (c).

show that age structure allows for a broad influence of the activist population: age differentiation allows activists to persist over different age windows and not be depleted all at once by joining the radical pool. Thus, while still maturing toward full-fledged radicalization, activists keep recruiting members into their ranks through peer pressure, continuously funneling individuals to the radical state.

If we further increase $C_R = 50$ ($c_R = 25$), as shown in Figure 7(c), we observe that, due to the very large radicalization rate, the activist fraction $n_1(t)$ is quickly depleted even within the age-dependent model. The loss of the intermediate activist population represents a bottleneck hindering radical population growth, as new members are no longer being recruited. As a result, even with a higher radicalization rate, the $n_2(t \to \infty)$ steady states in this case are lower than in Figure 7(b) in both the age-dependent and age-independent models. In particular, in the age-independent formulation, the system will irreversibly settle along the $n_0^* + n_2^* = 1$ solution family, and not at the turmoil state. On the other hand, as can be seen in the dynamics of the age-dependent $n_2(t)$ in Figure 7(c), the continuous presence of radicals becomes unsustainable without activists supplying new recruits. Here, radicals eventually fade away due to old age and are replaced by non-radicals, under the population conservation conditions assumed in our model. This depletion slows the further radicalization of activists, who interact less with full-fledged radicals, allowing $n_1(t)$ to recover, as can be seen in the resurgent spike of activists in Figure 7(c). The rise in $n_1(t)$ triggers the regrowth of $n_2(t)$, which once again depletes the activist pool, leading to oscillations in $n_1(t)$ and $n_2(t)$ over time. During the second radicalization wave (and other hypothetical ones beyond the 100 years considered in this panel), the $n_1(t), n_2(t)$ populations reach higher values than during the first, transient one. Interestingly, the emergence of activists is seen to precede that of radicals by roughly five years, on the same time-scale as reported for a demographic study of individuals progressing from initial radicalization to full extremism (Klausen et al., 2016).

In Figure 8, we plot long-term population fractions $n_i(t = 100)$ for $i = 1, 2$ as a function of C_R ($c_R = C_R/2$) for the two formulations of our model. For low $C_R \lesssim 1$, radical fractions $n_2(t = 100)$ are negligible while activist populations $n_1(t = 100)$ remain close to metastable levels. These are slightly higher in the age-dependent case than in the age-independent one, as discussed above. Increasing radicalization rates to moderate $1 \lesssim C_R \lesssim 10$ values drives the age-independent model to the c_R-independent turmoil steady state at $(n_0^* = 5/6, n_1^* = 0, n_2^* = 1/6)$, where n_1^* vanishes. In contrast, within the age-dependent model, $n_1(t = 100)$ decreases with increasing C_R but stays non-zero, leading to a significantly elevated $n_2(t = 100)$ as discussed above. We find that there exists an optimal C_R^{opt} value that maximizes $n_2(t = 100)$ in the age-dependent case. Values of C_R that are too low hinder recruitment from the activist pool; values of C_R that are too large overtax, leading to an optimal C_R^{opt} value. As $C_R \gtrsim 10$ is further increased, $n_1(t = 100)$ continues to decline in the age-dependent model. Eventually, the oscillatory regime is reached, as shown in Figure 8. The age-independent model does not exhibit
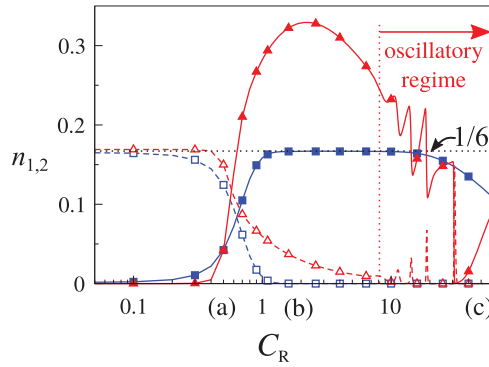
Figure 8. Long-time $n_1(t = 100)$ and $n_2(t = 100)$ populations as a function of C_R ($c_R = C_R/2$) for the age-independent and age-dependent models. The C_R values used in Figure 7 are explicitly marked. At low C_R, the radical population n_2 is negligible, and the activist population n_1 saturates. At intermediate C_R, the n_2 radicals rise by converting more n_1 activists. Note that $n_1(t = 100) \to 0$ in the age-independent case, while in the age-dependent model $n_1(t = 100)$ remains finite and leads to an enhanced radical population. At high C_R, the age-structured model yields oscillatory dynamics as shown by the spiky curves. In the age-independent model, $n_2(t = 100)$ declines as the system evolves toward the solution family $n_0^* + n_2^* = 1$ and away from turmoil at $n_2^* = 1/6$.

oscillations for large C_R; however n_2^* declines, indicating that turmoil is no longer reached, and that the system settles along the solution family $n_0^* + n_2^* = 1$ as described at the end of subsection III A.

In Figure 9, we show the age distribution of activists and radicals at long times ($t = 100$) under irreversible radicalization $C_P = 0$ using the same parameters as in Figure 7(b,c). We do not display the age distribution profiles corresponding to Figure 7(a) since the system is not equilibrated at $t = 100$ and the age distribution curves would be qualitatively similar to the short time ones corresponding to Figure 7(b).

In Figure 9(a), we use the same parameters as in Figure 7(b). For the activist age distribution $\rho_1(a, t \to \infty)$, a peak arises at age $a^* < \alpha_A$, and the distribution is similar to what observed in Figure 6(c) under reversible radicalization. Although the parameters are different, the mechanism leading to the early maximum in Figure 9(a) is the same as what outlined when discussing Figure 6 (c): namely activists quickly joining the rank of radicals as they mature, yielding an early age peak. In contrast, due to the irreversible nature of radicalization, the age distribution of radicals $\rho_2(a, t \to \infty)$ increases continuously until a plateau is reached since, once radicalized, individuals can only age within the extremist pool but not deradicalize.
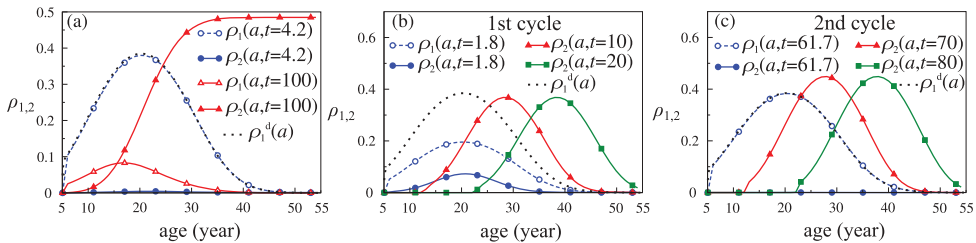

Figure 9. Age distribution of activists and radicals for the parameters used in Figure 7(b,c). In panel (a), activists emerge first, and at $t = 4.2$, their age distribution is close to the dormant distribution $\rho_1^d(a)$. At long times ($t = 100$ years) radicals surpass the activist population. Their age distribution increases at young ages and plateaus at older ones. A small fraction of activists remains, peaking at ages younger than a_A. Panel (b) depicts the age distributions during the transient phase of the oscillatory regime. At $t = 1.8$ activists reach a maximum, and a small radical fraction emerges. At $t = 10$ and 20 the activist population (not plotted) vanishes, while that of radicals increases. The age distribution of radicals maintains its shape as it advects toward older ages. Panel (c) shows the age distributions of the oscillatory regime after the transient period. Behaviors are qualitatively similar to panel (b). However, when activists reach a maximum at $t = 61.7$ years, the radical population remains negligible, allowing activists to approach the dormant state and increasing the radical population at $t = 70$ and 80.

In Figure 9(a), we also plot the age distributions at $t = 4.2$ when the fraction of activists $n_2(t = 4.2)$ is at the maximum value shown in Figure 4(b). For comparison, we also show the $\rho_1^d(a)$ distribution obtained by forcing $\rho_2(a, t) = 0$ while numerically solving Equations 1–6. Because this constraint allows only non-radicals and activists to arise, $\rho_1^d(a)$ may be used as a proxy for the age distribution of activists at the dormant state; we can also interpret $\rho_1^d(a)$ as the age-dependent analogue of the dormant solution discussed for the age-independent model in subsection III.A. As can be seen from Figure 9(a), the $\rho_1(a, t = 4.2)$ and $\rho_1^d(a)$ distributions are almost identical, suggesting that the system transitions through the dormant state while evolving from utopia to turmoil, similarly as to what observed in the age-independent case, as discussed in Figure 3(c). As mentioned above, the age distributions corresponding to Figure 7(a) at $t = 100$ would look qualitatively similar to $\rho_i(a, t = 4.2)$ for $i = 1, 2$ in Figure 9(a).

The parameters used in Figure 7(c) lead to oscillatory behavior. Since a long-term steady state cannot be identified, we plot the age distributions at times of interest. We begin with $t = 1.8$ when the activist population reaches its first maximum, corresponding to the early peak in Figure 7(c), and the radical population has increased to appreciable values. In Figure 9(b) the age distributions for both populations peak near ages $a \simeq \alpha_A = \alpha_R = 20$, with $\rho_1(a, t = 1.8) \ll \rho_2(a, t = 1.8)$ for all ages. At later times, as the number of radicals increases, the number of activists decreases to almost extinction. In Figure 9(b), we also plot $\rho_2(a, t = 10)$ and $\rho_2(a, t = 20)$. Their shape is almost identical and $\rho_2(a, t = 20) \simeq \rho_2(a + 10, t = 10)$ since within this time frame radicals can only age, but neither increase nor decrease, as the activist pool is depleted, and radicalization is irreversible. Eventually, at $a = a_1$, radicals age out of the system, repopulating first the non-radical, and subsequently the activist pool. A second oscillation cycle begins.

In Figure 9(c), we plot the age distributions beginning at $t = 61.7$, when the activist fraction reaches the second maximum shown in Figure 7(c). Here the radical population is vanishingly small, while the activist age distribution is very close to that of dormant state. The two behaviors at $t = 1.8$ and $t = 61.7$ are different, due to initial conditions. In particular, we note that at the onset even the small, uniform, radical population $\rho_2(a, t = 0) = 0.001$ is able to funnel non-radicals toward full-fledged extremism, bypassing the dormant state. A large number of radicals quickly consolidates. This initial condition effect damps away after a transient period, when the number of radicals declines due to aging and the non-radical population is replenished. As the cycle begins anew with almost no radicals, the system is able to reach the dormant state, with a large activist population. Eventually, the latter radicalizes, yielding the age distribution $\rho_2(a, t = 70)$ depicted in Figure 9(c). The above dynamics show that while at short times the initial radical population serves as a conduit to early, large-scale radicalization, it also causes the rapid depletion of the activist pool, until recruits are no longer available, halting further radicalization. On the other hand, in the second cycle, with a vanishingly small initial radical population, activists are better able to increase their ranks and in turn to sustain a continuous transition toward the final radical stage. Indeed, the total number of radicals in the second cycle from both Figure 7(c) and Figure 9(c) is much larger than in the first cycle. The early emergence of radicals may thus be counterproductive. Advection is still observed as $\rho_2(a, t = 80) \simeq \rho_2(a + 10, t = 70)$.

We now examine how other parameters influence the long-term radical population. In Figure 10(a), we plot $n_2(t = 100)$ as a function of C_A/C_D and C_R/C_D. In general, C_A/C_D is seen to dictate whether a radical population may ever arise, while C_R/C_D determines long time behavior and whether a steady or an oscillatory state is reached. The $n_2(t = 100)$ population increases with increasing C_A/C_D and reaches a maximum at $C_R/C_D \simeq 0.5$ regardless of C_A/C_D. As discussed above, $n_2(t = 100)$ has not reached steady state for smaller C_R/C_D and is hampered by over-drainage of the activist pool for larger C_R/C_D. Finally, for large C_R/C_D oscillatory behavior arises, as indicated by the striped pattern in the upper-right portion of Figure 10(a). Reducing C_A/C_D hinders the activation of non-radicals and may be considered a prevention strategy; in contrast, reducing C_R/C_D impedes full radicalization and may be considered a correctional strategy. The results from Figure 10(a) suggest that prevention may be more effective than correction. To convey this point, we highlight a line of constant $C_A/C_D +$
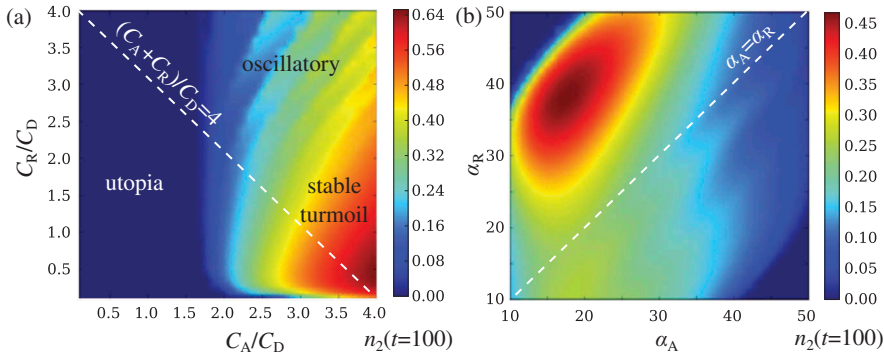
Figure 10. Long-time $n_2(t = 100)$ radical population as a function of C_A/C_D and C_R/C_D in panel (a) and α_A and α_R in panel (b). In panel (a) $n_2(t = 100)$ is negligible until $C_A/C_D \gtrsim 2$, after which it increases. As a function of C_R/C_D, $n_2(t = 100)$ peaks at $C_R/C_D \simeq 0.5$; further increases lead to a decline and to oscillatory behavior. In panel (b) $n_2(t = 100)$ peaks at $\alpha_A \simeq 15$ and $\alpha_R \simeq 35$. Starting from the maximum, $n_2(t = 100)$ drops sharply by increasing α_R and gradually by increasing α_A. Unless being varied, parameters are $C_D = 5$, $C_A = 12$, $C_R = 8$, $\alpha_A = \alpha_R = 20$, and $\sigma_A = \sigma_R = 10$.

$C_R/C_D = 4$ to represent a scenario where total escalation rates rates are constant but can be preferentially directed toward activation or radicalization. Under this constraint, lowest values of $n_2(t = 100)$ are found by decreasing C_A/C_D; although the corresponding radicalization rate is large, the activist pool is too small to yield a sizable radical population.

Figure 10(b) shows the steady state radical population as a function of α_A and α_R. The maximum of $n_2(t = 100)$ is located at $\alpha_A \simeq 17$ and $\alpha_R \simeq 38$, suggesting that radicalization is most pronounced when non-radicals are activated in their late teens and the resultant activist pool is given ample time to develop. The large age difference between α_A and α_R allows the age stratified activists to most effectively funnel non-radicals to the radical pool. Although such large values of α_R are not realistic Figure 10(b) implies that, given an activation age α_A, the number of radicals increases with radicalization age α_R, allowing the activist pool to keep sustaining radical growth. This growth continues until α_R reaches large values (here, roughly 40), when the various populations no longer overlap in age, and the interaction kernel $K(a, a'; \alpha_R, \sigma_R)$ loses its effectiveness.

So far, we have analyzed expected outcomes over long times. In particular, we find that age dependence allows for the asymptotic emergence of utopia, a dormant state and turmoil, just as in the age-independent formulation. However, the basins of attraction of these steady states and the associated populations may differ greatly in the two formulations. For example, the strong promotion of radicalization at early ages may lead to a premature draining of the activist pool, effectively thwarting further radicalization. In this context, the radical ideology spreads too quickly among a few who become isolated from the rest of society and who are not able to effectively recruit more adherents through peer pressure at the intermediate, activist stage. Most notably, in certain parameter regimes, age structure allows for cyclic behavior to arise with alternating waves of more or less radicalized individuals. The above-described trends often arise over several years, when the system has equilibrated. In more practical situations, however, interventions may have been introduced earlier, before reaching the above steady state predictions. We thus turn our attention to short-time phenomena, at the onset of an escalating situation.

C. Short-time behavior

As outlined in the previous subsection, starting from a quasi-utopia initial configuration, the dynamics of the system evolves over two stages. Activists emerge first and reach a metastable, finite population; radicals remain few. In the second phase, activists turn into radicals, and the metastable state is dissipated. In this subsection, we use perturbation theory to examine the onset of the activist population from an initial non-radical society and the onset of the radical population from the activist pool.

We begin by perturbing utopia, defined as $\rho_i(a) = 1$ for $i = 0$ and $\rho_i(a) = 0$ for $i = 1, 2$, and examine how trajectories depart from it. An age-dependent perturbation around utopia can be expressed as $\rho_1(a, t) = \delta\rho_1(a, t)$, $\rho_2(a, t) = \delta\rho_2(a, t)$, and $\rho_0(a, t) = 1 - \delta\rho_1(a, t) - \delta\rho_2(a, t)$, where $\delta\rho_1(a, t), \delta\rho_2(a, t) \ll 1$ are small perturbations. The age structures at $t = 0$ are given as $\delta\rho_i(a, t = 0)$ for $i = 1, 2$. Upon linearizing the system to first order we find that for short times

$$\frac{\partial\delta\rho_1}{\partial t} + \frac{\partial\delta\rho_1}{\partial a} = A(a; \delta\rho_1) - C_D\delta\rho_1, \tag{15}$$

$$\frac{\partial\delta\rho_2}{\partial t} + \frac{\partial\delta\rho_2}{\partial a} = 0, \tag{16}$$

where $A(a; \delta\rho_1)$ is given by Equation 4. The perturbations do not contribute to the boundary condition in Equation 7 since their sum is zero by construction. Equation 16 implies that $\delta\rho_2(a, t)$ retains its original age structure and is simply advected in time. The radical population remains small for short times as expected. Since it is linear in $\delta\rho_1$, Equation 15 can be recast in terms of an age-dependent operator $\mathcal{L}(a)$ defined as

$$\frac{\partial\delta\rho_1}{\partial t} = \mathcal{L}(a)\delta\rho_1. \tag{17}$$

The growth of an initially infinitesimally small $\delta\rho_1(a, t)$ can be approximated as $\delta\rho_1(t, a) \sim \exp(\lambda_u t)\phi_1^u(a)$, where λ_u is the largest eigenvalue arising from Equations 17 and $\phi_1^u(a)$ is its corresponding eigenfunction. We can interpret λ_u as the onset growth rate of activists: $\lambda_u < 0$ implies a regression of activists toward utopia and characterizes utopia as stable, whereas $\lambda_u > 0$ indicates departure from utopia and characterizes utopia as unstable. Unless otherwise stated or varied, parameters are chosen here as $C_A = 12$, $C_D = 5$, $C_R = 2$, $\sigma_A = \sigma_R = 10$, $\alpha_A = \alpha_R = 20$, as used in Figure 7(b). We numerically compute the largest eigenvalue λ_u and its corresponding eigenfunction $\phi_1^u(a)$ using the power method (Bodewig, 1956; Golub & Van Der Vorst, 2000; Von Mises & Pollaczek-Geiringer, 1929). Here, the given operator is applied to an arbitrary initial function; the result is normalized and reapplied to the same operator. The process is iterated until input and output converge.

In Figure 11(a), we plot λ_u as a function of C_A/C_D and σ_A, the relative intensity and width of the activation rate. For low values of C_A/C_D, λ_u is negative: perturbations vanish and utopia is stable. Higher values of C_A/C_D lead to positive λ_u and to large-scale instabilities. The marginal stability line at $\lambda_u = 0$ separates the two regimes. The unstable region expands with decreasing σ_A, suggesting that non-zero activist configurations may be more easily reached by narrowing the age range in the interaction kernel $K(a, a'; \alpha_A, \sigma_A)$ while at the same time increasing its peak by construction. Larger σ_A values spread the kernel over a large age range, resulting in a modest peak that may not be enough to sustain activist growth. As expected, λ_u increases with C_A/C_D. Other parameters α_A, C_R, σ_R, and α_R have negligible effects.

The eigenfunction $\phi_1^u(a)$ represents the age-differentiated growth amplitude of activists and is shown in Figure 11(b) for three σ_A values. As is evident for increasing α_A, $\phi_1^u(a)$ peaks at $a \gtrsim \alpha_A$, not at $a = \alpha_A$. This can be explained by recalling that activist populations increase with age because we initiate our system from a quasi-utopia state, and because our chosen boundary conditions in Equations 7 and 8 preferentially repopulate the non radical state at age $a = a_0$. Because the interaction kernel $K(a, a'; \alpha_A, \sigma_A)$ favors interactions between same-age individuals, non-radical early adults, slightly older than $a = \alpha_A$, are more likely to interact with activists of their same age than with non-radicals, as activists are simply more numerous at this age. Hence, there is a higher likelihood that young non-radical adults older than $a = \alpha_A$ become activated due to societal interactions. The peak of $\phi_1^u(a)$ is shifted further to the right as the range of social interactions increases, that is, for larger values of σ_A. Of course, this outcome depends on the specific choice for $K(a, a'; \alpha_A, \sigma_A)$. Finally, as can be seen, $\phi_1^u(a)$ becomes wider and shallower with increasing σ_A, until, for $\sigma_A \to \infty$, $\phi_1^u(a \gg a_0)$ is constant, except for $\phi_1^u(a \simeq a_0)$, where boundary conditions pin it close to zero.

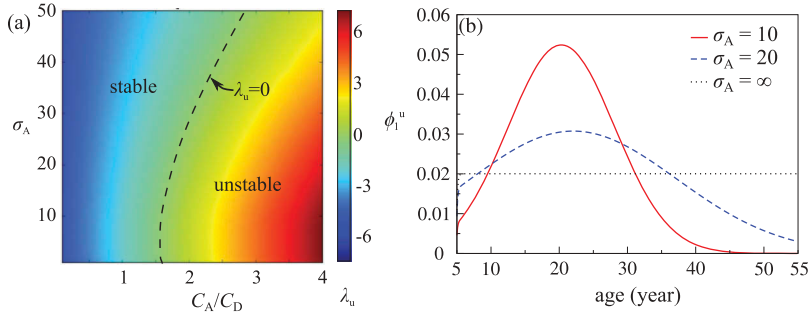**Figure 11.** Perturbations around utopia. (a) Activist growth rate λ_u as a function of C_A/C_D and σ_A. The eigenvalue λ_u decreases with increasing C_A/C_D and decreasing σ_A, suggesting that kernels tightly clustered in age magnify the instability of utopia. (b) The age-differentiated growth amplitude $\phi_1^u(a)$, the eigenfunction corresponding to λ_u, for various σ_A with $C_A/C_D = 2.4$ and $a_A = 20$. As σ_A increases, the peak of $\phi_1^u(a)$ shifts toward $a > a_A$ and its width increases as described in the text. For even larger σ_A, $\phi_1^u(a)$ is quasi-constant with the exception of the region $a \simeq a_0$, where the boundary condition suppresses activist growth by enhancing the non-radical pool. Unless being varied, parameters are $C_A = 12$, $C_D = 5$, $C_R = 5$, $a_A = 20$.

In the unstable case, when $\lambda_u > 0$, perturbations around utopia grow and drive the system toward the dormant steady state. Note that $\phi_1^u(a)$ shown in Figure 11(b) for $\sigma_A = 10$ and $\rho_1^d(a)$ shown in Figure 9(c) have similar profiles, suggesting that as the system evolves from utopia to the dormant state, the $\phi_1^u(a)$ eigenfunctions grow uniformly toward $\rho_1^d(a)$.

At longer times, the system leaves the dormant region and progresses toward the turmoil state. We similarly investigate the short-term behavior of this process using perturbation analysis. In particular, we reset time so that at $t = 0$ the system is in the dormant state and model small fluctuations as $\rho_1(t, a) = \rho_1^d(a) + \delta\rho_1(t, a)$, $\rho_2(t, a) = \delta\rho_2(t, a)$, and $\rho_0(t, a) = 1 - \rho_1^d(a) - \delta\rho_1(t, a) - \delta\rho_2(t, a)$, where the perturbations $\delta\rho_1(a, t), \delta\rho_2(a, t) \ll 1$ for all ages and for short times. Upon substitution into Equations 1–3, and linearizing to first order, we find

$$\frac{\partial\delta\rho_1}{\partial t} + \frac{\partial\delta\rho_1}{\partial a} = -A(a; \rho_1^d)\big(\delta\rho_1 + \delta\rho_2\big) - C_D\delta\rho_1 \tag{18}$$

$$+ A(a; \delta\rho_1)\big(1 - \rho_1^d\big) - R(a; \delta\rho_2)\rho_1^d,$$

$$\frac{\partial\delta\rho_2}{\partial t} + \frac{\partial\delta\rho_2}{\partial a} = R(a; \delta\rho_2)\rho_1^d. \tag{19}$$

As done above, we also approximate the growth of the perturbation near the dormant state as $\delta_i(t, a) \simeq \exp(\lambda_d t)\phi_i^d(a)$, where λ_d is the largest eigenvalue of the operator stemming from Equations 18 and 19 and represents the growth rate of radicals near the dormant state. The corresponding eigenfunctions are $\phi_i^d(a)$ with $i = 1, 2$.

In Figure 12(a), we plot λ_d as a function of C_R/C_D and σ_A. As can be seen, the dormant state is always unstable: in the absence of a pacification mechanism, radicals will never return to the activist stage. In Figure 12(b), we analyze the dependence of λ_d on α_R and α_A. We find that λ_d reaches a maximum for $\alpha_R \gtrsim \alpha_A$, at approximately the same age when the activist distribution in the dormant state $\phi_1^d(a)$ also reaches a maximum. Thus, radicalization may be greatly enhanced by targeting the ages corresponding to the largest activist population. It is interesting to note that the long-term behavior of $n_2(t = 100)$ and the short-term radical growth rate λ_d depend on α_A and α_R in very different ways, as can be seen by comparing Figure 10(b) and 12(b). At short times, Figure 12(b) shows that λ_d is largest for $\alpha_R \simeq \alpha_A$; at longer times, 10(b) reveals that $n_2(t = 100)$ is largest for $\alpha_R > \alpha_A$. These results indicate that although the instability is initially largest when the two target ages are similar, the choice of $\alpha_R \simeq \alpha_A$ drains the activist pool too quickly for radicals to achieve long term growth. Radical populations are largest when the two
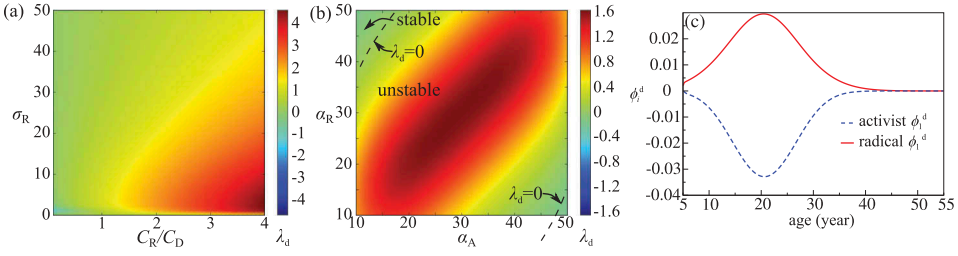
Figure 12. Perturbations around the dormant state. (a) Radical growth rate λ_d as a function of C_R/C_D and σ_R. The dormant state is mostly unstable since λ_d is always positive. (b) Radical growth rate λ_d as a function of a_A and a_R. λ_d is greatest near the $a_A = a_R$ line. Small patches of stable regimes occur when a_R and a_A differ greatly. (c) Normalized growth patterns of activists $\phi_1(a)$, and radicals, $\phi_2(a)$. Radicals increase at the expense of activists, since $\phi_2(a) > 0$ and $\phi_1(a) < 0$. Unless varied, parameters are $C_A = 12$, $C_R = 8$, $a_{A,R} = 20$, $\sigma_{A,R} = 10$, $C_D = 5$, $\sigma_D \to \infty$.

target ages are different allowing for the age-structured interactions to optimally funnel populations to the radical state.

In Figure 12(c), we compute the eigenfunctions $\phi_1^d(a)$ and $\phi_2^d(a)$ for $C_R/C_D = 0.4$, with the other parameters as detailed above. These eigenfunctions represent the age-differentiated growth amplitudes of activists and radicals, respectively. Numerically, we find $\lambda_d = 0.37$. A positive $\phi_2^d(a)$ and a negative $\phi_1^d(a)$ emerge, indicating growing radical and decreasing activist populations, as expected. However, $\phi_2^d(a)$ does not exactly match $-\phi_1^d(a)$: the latter exceeds the former at young ages, implying that a fraction of activists returns to the non-radical status. At old ages, $\phi_2^d(a)$ exceeds $-\phi_1^d(a)$, suggesting that non-radicals are activated, and subsequently radicalized, spurring further radicalization. As the system evolves away from utopia or the dormant state, a governmental agency may intervene to stem radicalization through age-based educational or rehabilitation programs. In the next section, we explore the effects of age-dependent intervention.

Government intervention

To study the effects of government sponsored programs, we consider a population that undergoes radicalization from an initial utopia and irreversibly. We model intervention in the form of age-dependent conversion terms that lower extremist levels incrementally, converting radicals to activists, or activists to non-radicals. We thus re-write the previously uniform de-escalating terms C_D and $C_P = 0$ in Equations 1–3

$$C_D \to C_D + \mu G(a), \tag{20}$$

$$C_P = 0 \to (1 - \mu) G(a), \tag{21}$$

where $0 \le \mu \le 1$ determines how efforts are divided between the two possible intervention avenues. Relatively large μ implies that most resources are focused on returning activists to the non-radical state, while more modest μ values represent intervention in returning radicals to the activist state. The age dependent term $G(a)$ is modeled similarly to the interaction kernels in Equation 6

$$G(a) = C_G \frac{\exp\left[-\frac{(\alpha_G - a)^2}{2\sigma_G^2}\right]}{\int_{-\bar{a}}^{\bar{a}} \exp\left[-\frac{s^2}{2\sigma_G^2}\right] ds}. \tag{22}$$
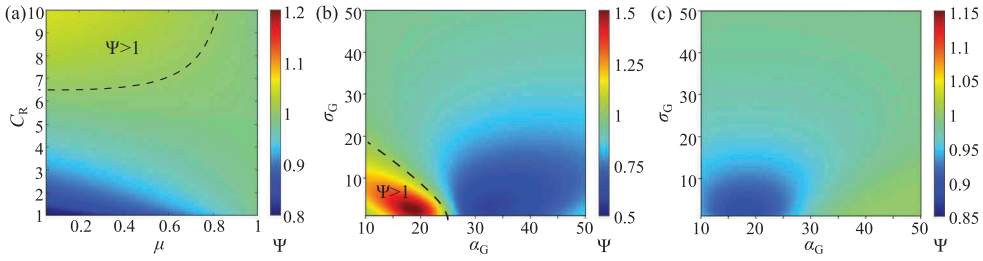
Figure 13. Government intervention. (a) Radical suppression ratio Ψ as a function of μ and C_R for $\alpha_G = \alpha_{A,R}$ and $\sigma_G = \sigma_{A,R}$. For strong radicalization (large C_R) Ψ decreases when μ increases, suggesting that activist prevention is more effective. For mild radicalization (low C_R), radical prevention is more advantageous. (b) Radical suppression ratio Ψ as a function of α_G and σ_G through the pacification of radicals, $\mu = 0$. Optimal reduction of radicals is achieved for $\alpha_G > \alpha_{A,R} = 20$. Intervention may be counterproductive for targeted ages $\alpha_G < \alpha_{A,R} = 20$. (c) Radical suppression ratio Ψ as a function of α_G and σ_G through the de-escalation of activists, $\mu = 1$. Optimal reduction of radicals is achieved for $\alpha_G < \alpha_{A,R} = 20$. Unless varied, parameter values are $C_A = 12$, $C_R = 10$, $C_D = 5$, $\alpha_{A,R} = 20$, $\sigma_{A,R} = 10$, and $C_G = 1$ for (a) and 5 for (b) and (c).

Here, C_G represents the intensity of intervention, and α_G and σ_G are the corresponding target age and spread. To quantify the effectiveness of intervention, we introduce a radical suppression ratio $\Psi \equiv n_2^G(t \to \infty)/n_2^T(t \to \infty)$ where $n_2^T(t \to \infty)$ is the steady state radical fraction at turmoil arising from Equations 1–6 and $n_2^G(t \to \infty)$ is similarly evaluated except for the government intervention substitutions in Equations 20 and 21. To be concrete, we select societal parameters as in Figures 7 and 8, $C_A = 12$, $C_D = 5$, $\alpha_A = \alpha_R = 20$, $\sigma_A = \sigma_R = 10$, initial conditions $\rho_0(a, 0) = 0.989$, $\rho_1(a, 0) = 0.01$, $\rho_2(a, 0) = 0.001$, and vary C_R. Since Ψ is meaningful only if $n_2^G(t \to \infty)$ and $n_2^T(t \to \infty)$ converge to unique values, we limit the $C_R \leq 10$, before the oscillatory regime shown in Figure 8 is reached. Government intervention is introduced once society has reached steady state.

As expected, Ψ decreases with C_G, indicating that larger intervention leads to the emergence of less radicals. In Figure 13(a), we fix $C_G = 1$, $\alpha_G = \alpha_R = \alpha_A$, $\sigma_G = \sigma_R = \sigma_A$, and plot Ψ as a function of μ and C_R. For small values of C_R, Ψ decreases with μ; the trend is reversed for large C_R. This suggests that if the push toward radicalization is mild, at low C_R, the most effective intervention is to aim resources at pacification, returning radicals to the activist state. Decreasing the number of radicals will lessen their influence on potential recruits. Vice-versa, for strong radicalization under large C_R, the optimal strategy is to encourage activists to return to the non-radical stage, preventing radicalization at its incipit. We also note that Ψ increases with C_R, indicating that the more aggressive radicalization is, the harder it is to suppress radicals. Finally, when C_R is large and $\mu \to 0$, Ψ can increase beyond unity: government intervention enhances radicalization. The mechanism behind this unwanted outcome is that fostering the return of radicals toward the activist state yields a much enlarged activist pool that is able to recruit more non-radicals into the process. The net result is that the number of radicals will increase. This effect is magnified for large C_R, when activists quickly turn into radicals, and the activist pool becomes a scarcely populated bottleneck. Government intervention enlarges the activist pool, alleviating the bottleneck, and fortuitously aiding the conversion of radicals. We do not observe the same result at small C_R since there is no bottleneck and activists are quite numerous even before intervention.

In Figure 13(b,c), we set $C_R = 10$ and $C_G = 5$ and plot Ψ as a function of the characteristic ages α_G and σ_G for $\mu = 0$ in panel (b) and $\mu = 1$ in panel (c). Only values of $\sigma_G \lesssim 10$ affect Ψ, which may be expected since the age-dependent model converges to the age-independent one as $\sigma_G \to \infty$. In Figure 13(b), where $\mu = 0$, $\Psi > 1$ for $15 \lesssim \alpha_G \lesssim 25$ and $\alpha_A = 20$, implying government intervention is counterproductive, as outlined above. Vice-versa, Ψ is lowest for $30 \lesssim \alpha_G \lesssim 45$ when radicals who return to the activist pool interact less with younger non-radicals. In Figure 13(c), where $\mu = 1$, $\Psi < 1$ for all values of α_G and σ_G and its lowest value is within $15 \lesssim \alpha_G \lesssim 25$.

Discussion

Several population dynamics models have been proposed to study multistage radicalization (Camacho, 2013; Castillo-Chavez & Song, 2003; Deutscha & Ehrhard, 2015; Ehrhardt et al., 2013; Marvel et al., 2012; Santonja et al., 2008). Our work shows that including age dependence, even in the simplest form of interactions between populations, can lead to rich dynamics, enhancing radicalization in certain parameter regimes, and leading to oscillatory behavior. Age-independent radicalization models generally converge to fixed ratios among populations, and phase portraits do not display limit cycles (Castillo-Chavez & Song, 2003; Deutscha & Ehrhard, 2015), as shown here for the age-independent formulation of our model. Yet, according to one of the most influential theories of terrorism, developed by the political scientist D. C. Rapoport, extremist tendencies rise and fall over time like waves or ripples (McAllister & Schmid, 2011; Parker & Sitter, 2016; Rapoport, 2002; Sedgwick, 2007). Our age-structured model provides a potential mechanism to explain such wave-like behavior. In particular, we predict oscillatory solutions when i) radicalization is aggressive (C_R is large) and ii) radicalization is irreversible ($C_P = 0$). As shown in Figure 7 (c), the typical timescale for sustained radical populations is roughly 40 years, in agreement with sociological observations (McAllister & Schmid, 2011; Parker & Sitter, 2016; Rapoport, 2002; Rasler & Thompson, 2009; Sedgwick, 2007). The lifetime of these radical states depends on the age interval $[a_0, a_1]$ within which existing radicals are able to convert non-radicals. This finding supports Rapoport's conjecture that extremists radicalize a generation of individuals, and when their influence fades due to aging, the cycle of terrorism comes to an end (McAllister & Schmid, 2011; Rapoport, 2002). Recent studies using data analysis to quantitatively inspect Rapoport's wave theory have observed a relatively shorter lifespan of about 30 years for the so-called "New Left" terrorist wave emerging from Marxist movements (Rasler & Thompson, 2009). This observation is consistent with a smaller effective age interval of influence in our model and can be justified by noting that Marxism is a relatively more sophisticated ideology, compared to religious or nationalist fanaticism. Indoctrination of younger individuals may thus be less effective because their understanding of socioeconomic issues may still be under development. Quantitative studies have been facilitated by the creation of dedicated databases to index terrorist related data starting from the 1960s (Bogen & Jones, 2005; LaFree & Dugan, 2007). Prior records are sparse, and the data is not sufficient for quantitative analysis of radical resurgence within a society and over long periods of time, as would be required to validate the existence of generational waves predicted by our model. Global data, such as fatalities in conflicts over the past several centuries, do exhibit oscillatory patterns with a period of roughly half a century (Roser, 2018); however, lumping together data from various parts of the world may not be directly applicable to our model, due to the great regional variability and the limited information spread of centuries past. From a more qualitative perspective, religion-driven conflicts seem to display signs of ebbs and flows throughout history at regional scales. For examples, the 13th century Crusades in Europe were followed by the Renaissance, a relatively peaceful era, and again by the 16th century protestant Reformation wars. Similarly, in the Middle East, the 19th century Islamic revival inspired anti-colonial wars; religious leaders were later replaced by secular authorities who ruled for most of the 20th century, until they were toppled or threatened by religious movements. Notably, the worldwide decline of religious influence in the 20th century even led to the once prominent "secularization" theory (Chaves, 1994; Fox, 2012; Wald & Wilcox, 2006), according to which religions would continue fading and eventually disappear. However, religious fanaticism has returned with a vengeance in recent decades (Fox, 2012; Wald & Wilcox, 2006). Oscillatory phenomena can sometimes be observed within long-lasting conflicts, such as the struggle between Israelis and Palestinians, although counter-measures implemented in response to specific incidents can contribute to some short-term fluctuations as well (Such as data from B'Tselem: The Israeli Information Center for Human Rights in the Occupied Territories www.btselem.org/statistics/, and from Israel Ministry of Foreign Affairs) (Multiple sources, 2018). Admittedly, the real world is much more complicated than our model, and the evolution of human society will involve other factors that are not included in Equations 1–6. Notwithstanding, the oscillatory solutions of our model under fixed conversion intensities $C_{A/R/D}$ suggest the possibility of resurgence for a declining, or even inactive, ideological movement, provided that the underlying sociological contexts persist over time.

In addition to cyclic behavior, we also find that age structure increases the sensitivity of the dynamics to parameter values. For example, in Figure 8, the long-time radical fraction $n_2(t = 100)$ derived in the age-dependent model is nearly doubled by doubling C_R from 1 to 2, while the corresponding age-independent $n_2(t = 100)$ stays uniform. Moreover, as can be seen in Figure 10 (b), the age-dependent $n_2(t = 100)$ is highly sensitive to shifts in α_A and α_R, even if the magnitudes of the rates stay unchanged. These results indicate that age-dependent radicalization models can lead to more volatility and to more complex behavior compared to the more straightforward predictions arising from age-independent models. These nuances imply that governments can greatly improve the outcome of their interventions by targeting the right age groups rather than treating all ages the same way.

Finally, we find that the most effective tactic to reduce the radical population is to prevent activation by decreasing C_A as shown in Figure 10(a). From a practical perspective, this may be achieved by reducing the factors that lead to the activation of non-radicals through education, hope for the future, and employment. Sometimes, however, this may not be possible, and eliminating escalating factors for one group may lead another to radicalize. An alternate, corrective approach, may be to de-activate the activist population or to pacify radicals.

In cases where radicalization is very aggressive, the optimal intervention strategy is to reduce the number of activists, effectively isolating the most extreme from the general non-radical public. However, when radicalization is moderate, although the number of radicals is relatively small, a large body of activists will emerge, in response to an ideology that may be justified among the general public. In this case, the best intervention strategy is to focus on pacification, reducing the numbers of those who have taken the ideology to extreme levels. Current intervention policies are of two types: stopping extremists who are about to engage in violent activities, while allowing all freedom of speech is known as the "Anglo-Saxon" approach; preventing the spread of extreme views before violence arises is the "European" approach (Neumann, 2013). We can loosely interpret the choice of $\mu = 0$ in our intervention protocol to represent the Anglo-Saxon approach, where radicals are targeted, while $\mu = 1$ corresponds to the European approach, where the de-escalation of activists is sought. Our results suggest that discerning which strategy is best may depend on the aggressiveness of the radicalization process, embodied by C_R.

Conclusion

In this paper, we introduced a multistage radicalization model with age-structured progression rates. Upon comparison with the corresponding age-independent formulation, we find that age dependence leads to more complex, parameter-sensitive dynamics. In many cases, especially for irreversible radicalization, age dependence enhances the number of irreducible radicals. For large radicalization rates, age structure leads to oscillatory behavior, where large fractions of extremists ebb and flow over a lifetime of roughly 40 to 50 years. While the enhanced parameter sensitivity implies higher risks for escalation, it also provides an opportunity for effective policy making, for example, by surgically targeting more susceptible age groups. Upon comparing different government intervention strategies, we find that de-activation, that is, returning mildly indoctrinated individuals to the non-radical state, leads to more suppression of extremists when the radicalization rate is high. In the opposite case, the pacification of radicals may produce better results. Despite the great simplicity of the mathematical model, we observe a wide range of dynamical behaviors simply by distributing the strength of social interactions differently over age, without including more complicated external factors, such as the evolution of socioeconomic contexts or the change of political regimes. Sociologically, our findings suggest that the heterogeneity of social interactions among different age groups can profoundly change the course of progression, for example, the longevity and the pinnacle point, of an ideology within a population. Fundamentally distinctive phenomena can be overlooked if the effect of age structure is neglected and all age groups are lumped into a uniform population. It is particularly

interesting to note that the lifespan of radical activities in our oscillatory scenarios quantitatively agrees with the observed time scale in the wave theory of terrorism (McAllister & Schmid, 2011; Rapoport, 2002; Rasler & Thompson, 2009). Our model further suggests the potential for a past terrorist wave to resurge even after a long period of dormancy, unless the sociological contexts underlying the previous wave are sufficiently reduced to ensure the stability of a peaceful utopia.

Our model includes only three linear stages of radicalization. In particular, all non-violent steps are condensed in the intermediate activist stage, between the general non-radical population and the violence-prone extremists. We may increase the number of stages as done in previous age-independent work (Borum, 2003; Klausen et al., 2016; Moghaddam, 2005; Precht, 2007; Sageman, 2008; Wiktorowicz, 2004) for a more nuanced progression to radicalization, but we expect qualitatively similar results to what showed here for a linear pathway. Our model may be best used to approximate a slowly evolving society, where the populations are given sufficient time to relax toward quasistatic conditions, allowing higher order interactions, say, between ρ_0 and ρ_2, to dampen away, and a unique, primary pathway to emerge. Our findings can be very different from those arising in highly dynamical situations where multiple pathways exist to radicalization or more than two stages are nonlinearly coupled. For example, social interactions may exhibit "history" dependence, where the likelihood of radicalization may depend on the entire sequence of past states. Such history dependence may be directly incorporated in the transition rates between radicalization stages (Chuang, D'Orsogna, & Chou, 2017), or through the notion of social reinforcement, where transitions require multiple stimulations (Centola, 2010).

Furthermore, we assumed a constant total population with a uniform age distribution and have not included birth and death events (Chou & Greenman, 2016). Also not included is the possibility of forcefully removing individuals from the radical or activist pools, via arrest or involuntary exile. Neglecting birth and death may be a more suitable assumption for developed countries (Howden & Meyer, 2011), but for developing countries, especially in war-torn regions, birth and death rates are high and not balanced. Birth and death are known to have profound impact on the age structure of the overall population, leading to non-uniform age distributions (Boccara, Cheong, & Oram, 1994; Chou & Greenman, 2016; Keyfitz, 1997). Previous studies have connected the development of civil conflicts with a particular type of non-uniform age distributions known as the "youth bulge" where the population consists of disproportionately large youth cohorts (Fuller & Pitts, 1990; Hart, Atkins, Markey, Youniss, & Science, 2004; Hart et al., 2005). It is believed that youth bulge may intensify the competition for resource and employment opportunities, further exacerbating feelings of disaffection among the young (Farzanegan & Witthuhn, 2017; Mesquida & Wiener, 1999; Urdal, 2006; Yair & Miodownik, 2016). The effect of age-dependent birth and death has been studied under the same McKendrick-von Foerster framework presented here for various biological and ecological applications (Boccara et al., 1994; Chou & Greenman, 2016; Keyfitz, 1997; Leslie, 1945, 1948; McKendrick, 1925; Trucco, 1965) and can be added as an extension of our model to investigate youth bulge or related phenomena. While incorporating birth and death is beyond the scope of this paper, our current study can be used as a baseline for age-dependent social interactions, upon which further complexities may be added to describe more realistic scenarios.

Lastly, we present only the long-term outcome of government intervention policies, discussing what strategies may achieve the best results, regardless of implementation cost. Given limited resources, the best strategy may not always be possible, and so a utility function should be derived to seek an optimal balance between the cost of intervention and the gain from the prevention of radicalization. For example, a time-dependent utility function may allow the government to dynamically adjust its strategy based on past outcomes (Short et al., 2017; Short, Pitcher, & D'Orsogna, 2013).

Funding

References

Ahmed, A. G., Audu, D., Loza, W., & Maximenco, A. (2013). The prevalence of extreme Middle-Eastern ideologies among some Nigerians. *International Journal of Social Science Studies*, 1(2), 161–167.

Bakker, E. (2006). Jihadi terrorists in Europe, their characteristics and the circumstances in which they joined the Jihad: An exploratory study. *Technology reports*. Den Haag, The Netherlands: The Hague Clingendael Institute.

Boccara, N., Cheong, K., & Oram, M. (1994). A probabilistic automata network epidemic model with births and deaths exhibiting cyclic behaviour. *Journal of Physics A: Mathematical and General*, 27(5), 1585–1597.

Bodewig, E. (1956). *Matrix calculus*. Amsterdam, The Netherlands: North-Holland.

Bogen, K. T., & Jones, E. D. (2005). Risks of mortality and morbidity from worldwide terrorism: 1968–2004. *Risk Analysis*, 26(1), 45–59.

Borum, R. (2003). Understanding the terrorist mindset. *FBI Law Enforcement Bulletin*. 7–10.

Burton, T. (2005). *Volterra integral and differential equations*. New York, NY: Elsevier.

Camacho, E. T. (2013). The development and interaction of terrorist and fanatic groups. *Communications in Nonlinear Science and Numerical Simulation*, 18(11), 3086–3097. doi:10.1016/j.cnsns.2013.04.006

Castillo-Chavez, C., & Song, B. (2003). The development and interaction of terrorist and fanatic groups. In C. Castillo-Chavez (edited by), *Bioterrorism: Mathematical modeling applications in homeland security* (pp. 155–172). Philadelphia, PA: SIAM.

Centola, D. (2010). The spread of behavior in an online social network experiment. *Science*, 329(5996), 1194–1197. doi:10.1126/science.1185231

Chaves, M. (1994). Secularization as declining religious authority. *Social Forces*, 72(3), 749–774. doi:10.1093/sf/72.3.749

Chou, T., & Greenman, C. D. (2016). A hierarchical kinetic theory of birth, death and fission in age-structured interacting populations. *Journal of Statistical Physics*, 164(1), 49–76. doi:10.1007/s10955-016-1524-x

Chuang, Y.-L., D'Orsogna, M. R., & Chou, T. (2017). A bistable belief dynamics model for radicalization within sectarian conflict. *Quarterly of Applied Mathematics*, 75(1), 19–37.

Crenshaw, M. (2011). *Explaining terrorism: Causes, process, and consequences*. London, UK: Routledge.

Deutscha, T., & Ehrhard, M. (2015). Mathematical modelling of radicalization processes: The example of right-wing extremism in Germany. Submitted to Mathematical Social Sciences.

Doosje, B., Loseman, A., & van den Bos, K. (2013). Determinants of radicalization of Islamic Youth in the Netherlands: Personal uncertainty, perceived injustice, and perceived group threat. *Journal of Social Issues*, 69(3), 586–604. doi:10.1111/josi.2013.69.issue-3

Dumortier, F., Llibre, J., & Artés, J. C. (2006). *Qualitative theory of planar differential systems*. New York, NY: Universitext, Springer-Verlag.

Ehrhardt, M., Peco, M., Tarazona, A. C., Villanueva, R. J., & Villanueva-Oller, J. (2013). Popular support to terrorist organization: A short-term prediction based on a dynamic model applied to a real case. In J. C. Cortes, L. J. Sanchez, & R. J. Villanueva (edited by), *Mathematical modeling in engineering and social science*, (pp. 1–8). Hauppauge, NY: Nova Science Publishers..

Farzanegan, M. R., & Witthuhn, S. (2017). Corruption and political stability: Does the youth bulge matter? *European Journal of Political Economy*, 49, 47–70. doi:10.1016/j.ejpoleco.2016.12.007

Fox, J. (2012). The religious wave: Religion and domestic conflict from 1960 to 2009. *Civil Wars*, 14(2), 141–158. doi:10.1080/13698249.2012.679492

Fuller, G., & Pitts, F. R. (1990). Youth cohorts and political unrest in South Korea. *Political Geography Quarterly*, 9(1), 9–22.

Golub, G. H., & van der Vorst, H. A. (2000). Eigenvalue computation in the 20th century. *Journal of Computation and Applied Mathematics*, 123(1–2), 35–65. doi:10.1016/S0377-0427(00)00413-1

Hart, D., Atkins, R., Markey, P., Youniss, J., & Science, P. (2004). Knowledge, youth bulges, and rebellion. *Psychological Science*, 16(8), 661–662.

Horgan, J. (2008). From profiles to pathways and roots to routes: Perspectives from psychology on radicalization into terrorism. *The Annals of the American Association of Political and Social Sciences*, 618(1), 80–94.

Howden, L. M., & Meyer, J. A. (2011). Age and sex composition: 2010. Technology reports. Suitland, MD: United States Census Bureau.

Keyfitz, B. L. (1997). The McKendrick partial differential equation and its uses in epidemiology and population study. *Mathematical and Computer Modelling*, 26(6), 1–9. doi:10.1016/S0895-7177(97)00165-9

King, M., & Taylor, D. M. (2011). The radicalization of homegrown jihadists: A review of theoretical models and social psychological evidence. *Terrorism and Political Violence*, 23(4), 602–622. doi:10.1080/09546553.2011.587064

Klausen, J., Campion, S., Needle, N., Nguyen, G., & Libretti, R. (2016). Toward a behavioral model of "Homegrown" radicalization trajectories. *Studies in Conflict and Terrorism*, 39(1), 67–83 doi:10.1080/1057610X.2015.1099995

Koehler, D. (2014). Right-wing extremist radicalization process: The formers perspective. *Journal EXIT-Deutschland*, 1, 307–377.

LaFree, G., & Dugan, L. (2007). Introducing the global terrorism database. *Terrorism and Political Violence*, 19(2), 181–204.. doi:10.1080/09546550701246817

Leslie, P. H. (1945). On the use of matrices in certain population mathematics. *Biometrika*, 33(3), 183–212. doi:10.1093/biomet/33.3.183

Leslie, P. H. (1948). Some further notes on the use of matrices in population mathematics. *Biometrika*, 35(3/4), 213–245. doi:10.1093/biomet/35.3-4.213

Lofland, J., & Stark, R. (1965). Becoming a world-saver: A theory of conversion to a deviant perspective. *American Sociological Review*, 30(6), 862–875. doi:10.2307/2090965

Loza, W., El Fatah, Y. A., Prinsloo, J., Hesselink-Louw, A., & Seidler, K. (2011). *Journal of Interpersonal Violence*, 26 (3), 522–538.

Marvel, S. A., Hong, H., Papush, A., & Strogatz, S. H. (2012). Encouraging moderation: Clues from a simple model of ideological conflict. *Physical Review Letters*, 109(11), 118702. doi:10.1103/PhysRevLett.109.118702

McAllister, B., & Schmid, A. P. (2011). *The routledge handbook of terrorism research*. London, UK: Routledge. 210–293. chap. Theories of Terrorism.

McCauley, C., & Moskalenko, S. (2008). Mechanisms of political radicalization: Pathways toward terrorism. *Terrorism and Political Violence*, 20(3), 415–433. doi:10.1080/09546550802073367

McKendrick, A. G. (1925). Applications of mathematics to medical problems. *Proceedings of the Edinburgh Mathematical Society*, 44, 98–130.

Meeus, W. H. (2015). Why do young people become Jihadists? A theoretical account on radical identity development. *European Journal of Development Psychology*, 12(3), 275–281 doi:10.1080/17405629.2015.1024106

Mesquida, C. G., & Wiener, N. I. (1999). Male age composition and severity of conflicts. *Politics and the Life Sciences*, 18(2). 181–189. doi:10.1017/S0730938400021158

Moghaddam, F. M. (2005). The staircase to terrorism: A psychological exploration. *American Psychologist*, 60(2), 161–169.

Neumann, P. R. (2013). The trouble with radicalization. *International Affairs, 89(4), 873–893.* doi:10.1111/inta.2013.89. issue-4

Parker, T., & Sitter, N. (2016). The four horsemen of terrorism: It's Not Waves, It's Strains. *Terrorism and Political Violence*, 28(2), 197–216. doi:10.1080/09546553.2015.1112277

Precht, T. (2007). Home grown terrorism and Islamist radicalisation in Europe. *Technology reports*. Copenhagen, Denmark: Danish Ministry of Justice.

Rapoport, D. C. (2002). The four waves of rabel terror and September 11. *Anthropoetics: the Journal of Generative Anthropology*, 8(1), 1–19.

Rasler, K., & Thompson, W. R. (2009). Looking for waves of terrorism. *Terrorism and Political Violence*, 21(1), 28–41. doi:10.1080/09546550802544425

Roser, M. (2018). *War and peace, global deaths in conflicts since the year 1400 on our world in data (ourworldindata. org/war-and-peace), based on P. Brecke's conflict catalog at the centre for global economic history*. www.cgeh.nl/data

Sageman, M. (2004). *Understanding terrorist networks*. Philadelphia, PA: University of Philadelphia University Press.

Sageman, M. (2008). A strategy for fighting international islamist terrorists. *Annals of the American Academy of Political and Social Science*, 618(1), 223–231. doi:10.1177/0002716208317051

Santonja, F. J., Tarazona, A. C., & Villanueva, R. J. (2008). A mathematical model of the pressure of an extreme ideology on a society. *Computers and Mathematics with Applications*, 56(3), 836–846. doi:10.1016/j. camwa.2008.01.001

Sedgwick, M. (2007). Inspiration and the origins of global waves of terrorism. *Studies in Conflict and Terrorism*, 30(2), 97–112. doi:10.1080/10576100601101042

Seul, J. R. (1999). `Ours is the way of god': Religion, identity, and intergroup conflict. *Journal of Peace Research*, 36(5), 553–569. doi:10.1177/0022343399036005004

Short, M. B., McCalla, S. G., & D'Orsogna, M. R. (2017). Modelling radicalization: How small violent fringe sects develop into large indoctrinated societies. *Royal Society Open Science*, 4(8), 170678. doi:10.1098/rsos.170678

Short, M. B., Pitcher, A. B., & D'Orsogna, M. R. (2013). External conversions of player strategy in an evolutionary game: A cost-benefit analysis through optimal control. *European Journal of Applied Mathematics*, 24(1), 131-159. doi:10.1017/S0956792512000332

Silber, M. D., & Bhatt, A. (2007). *Radicalization in the west: The homegrown threat*. New York, NY: New York City Police Department.

Silke, A. (2003). Becoming a terrorist. In A. Silke (edited by), *Terrorists, victims, and society: Psychological perspectives on terrorism and its consequences*. Philadelphia, PA: Wiley.

Silke, A. (2008). Holy warriors. *European Journal of Criminology*, 5(1), 99–123. doi:10.1177/1477370807084226

Sprinzak, E. (1991). The process of delegitimation: Towards a linkage theory of political terrorism. *Terrorism and Political Violence*, 3(1), 50–68.

Trucco, E. (1965). Mathematical models for cellular systems: The von Foerster equation. Part I. *Bulletin of Mathematical Biophysics*, 27(3), 285–304.

Urdal, H. (2006). A clash of generations? Youth bulges and political violence. *International Studies Quarterly*, *50*(3), 607–629. doi:10.1111/isqu.2006.50.issue-3

Verma, G., Swami, A., & Chan, K. (2014). The impact of competing zealots on opinion dynamics. *Physica A: Statistical Mechanics and Its Applications*, *395*, 310–331.

Von Knop, K. (2007). Hypermedia seduction for terrorist recruiting. In B. Ganor, K. Von Knop, & C. Duarte (edited by), *NATO science for peace and security series E: Human and societal dynamics* (Vol. 25). Amsterdam, The Netherlands: IOS Press.

Von Mises, R., & Pollaczek-Geiringer, H. (1929). Praktische verfahren der gleichungsauflosung. *ZAMM - Zeitschrift Für Angewandte Mathematik Und Mechanik*, *9* 152–164.

Waagen, A., Verma, G., Chan, K., Swami, A., & D'Souza, R. (2015). Effect of zealotry in high-dimensional opinion dynamics models. *Physical Review E*, *91*(2), 022811. doi:10.1103/PhysRevE.91.022811

Wald, K. D., & Wilcox, C. (2006). Getting religion: Has political science rediscovered the faith factor? *American Political Science Review*, *100*(4), 523–529. doi:10.1017/S0003055406062381

Wiktorowicz, Q. (2004). *The roots of Islamic radicalism conference.* New Haven, CT: Yale University.

Multiple sources. (2018). *Such as data from B'Tselem: The Israeli Information Center for Human Rights in the Occupied Territories* www.btselem.org/statistics/, *and from Israel Ministry of Foreign Affairs*. http://mfa.gov.il/MFA/ForeignPolicy/Terrorism/Palestinian/

Yair, O., & Miodownik, D. (2016). Youth bulge and civil war: Why a country's share of young adults explains only non-ethnic wars. *Conflict Management and Peace Science*, *33*(1), 25–44.